General Disclaimer

One or more of the Following Statements may affect this Document

- This document has been reproduced from the best copy furnished by the organizational source. It is being released in the interest of making available as much information as possible.

- This document may contain data, which exceeds the sheet parameters. It was furnished in this condition by the organizational source and is the best copy available.

- This document may contain tone-on-tone or color graphs, charts and/or pictures, which have been reproduced in black and white.

- This document is paginated as submitted by the original source.

- Portions of this document are not fully legible due to the historical nature of some of the material. However, it is the best reproduction available from the original submission.

ANALYTICAL STUDY OF CONTROL DEVICES FOR HIGH AMPLITUDE COMBUSTION INSTABILITY

Samuel Z. Burstein

and

Harold Schechter

First Quarterly Report

to

National Aeronautics and Space Administration

Contract NAS 7-752

October 15, 1969

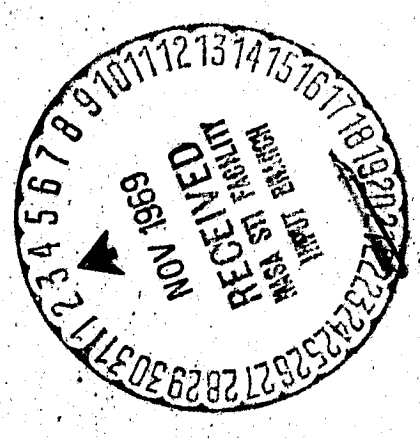

Mathematical Applications Group, Inc.

180 South Broadway

White Plains, New York

"This report contains information prepared by Mathematical Applications Group, Inc. (MAGI) under Contract NAS 7-752. Its content is not necessarily endorsed by the National Aeronautics and Space Administration."

TABLE OF CONTENTS

I. INTRODUCTION

This report describes the results of computer experiments being carried out on a numerical model of combustion processes in an annular rocket motor. The combustion process is controlled by an evaporation rate controlling mechanism but can be modified so as to include kinetic type energy release models. The model simulates numerically the complete nonlinear gas dynamic flow field in an annular motor. The coordinates are z, the axial length, θ, the angular coordinate, and time, t. This is the first model which is two-dimensional and time dependent which successfully includes the interaction of the combustion process with the nonlinear gas dynamic flow field. There have been[1,2] several analyses of a nonlinear form which come closest to modeling a physical combustion chamber[3] in which nonlinear effects are important. One could go to the literature[4,5] and obtain a rather complete introduction to linear theories of combustion instability. It has become apparent through the years that, although some qualitative aspects of the nonsteady combustion process can be described by a linear analysis, the degree of success that analysis will lend to design criterion in rocket engine technology clearly rests with nonlinear theory. Recent efforts[6] in this direction are appearing in the literature.

It is hoped that this report, which describes the continuation of an investigation in nonlinear rocket modeling, in [illegible] space dimensions, that was initiated with the Jet Propulsion Laboratories[7,8,9], will prove to be useful for analysis of stability limits in rocket motors which exhibit nonlinear behavior.

II. MODEL CONSIDERATIONS

The computer program TRDL represents a numerical model of an annular combustion chamber with coordinates of axial length z and angle θ. The combustor is assumed to be of negligible radial thickness $\Delta r << R$, R being the annular chamber's mean radius. Then the equations of motion are

$$\begin{aligned}
&\rho_t + (\rho u)_z + \tfrac{1}{R}(\rho v)_\theta = \dot{m} \\
&(\rho u)_t + (\rho u^2+p)_z + \tfrac{1}{R}(\rho uv)_\theta = 0 \\
&(\rho v)_t + (\rho uv)_z + \tfrac{1}{R}(\rho v^2+p)_\theta = 0 \\
&E_t + [(p+E)]_z + \tfrac{1}{R}[(p+E)v]_\theta = \dot{E}
\end{aligned} \tag{1}$$

where

$\rho = \rho(z,\theta,t)$ = mass/unit volume of combustion gas

$u = u(z,\theta,t)$ = velocity of combustion gas in axial direction

$v = v(z,\theta,t)$ = velocity of combustion gas in tangential direction

$E = E(z,\theta,t)$ = total energy/unit volume of combustion gas

To be more specific, the total energy is related to the internal energy/unit mass e and kinetic energy by

$$E \equiv \rho(e+\tfrac{1}{2}(u^2+v^2)) \tag{2}$$

The pressure may be eliminated as a variable through the equation of state

$$p = (\gamma-1)\rho e \ , \gamma = c_p/c_v \tag{3}$$

The inhomogeneous terms in the system of Equations (1) are the mass addition per unit volume per unit time $\dot{m}$, due to evaporation and combustion and $\dot{E}$ is the energy addition per unit volume per unit time associated with the mass addition.

In general, the dependence of these source terms are indicated by:

$$\dot{m} = \dot{m}(\rho,u,v,p;\text{drop parameters})$$

$$\dot{E} = \dot{E}(\rho,u,v,p;\text{ drop parameters}) \tag{4}$$

The components of the gas velocity, u and v, together with the drop velocity u_d and v_d determine the drag force acting on a drop. The magnitude of the force depends on the relative velocity. The components of the force in the axial and tangential direction is then related to the relative velocities through

$$\vec{F} = (F_z,F_\theta) \backsim ((u-u_d)^2 \cdot \text{sign}(u-u_d),(v-v_d)^2 \cdot \text{sign}(v-v_d)) \tag{5}$$

The introduction of this relative velocity appears from the dependence of the drag force experienced by the drop on the Reynolds number. The drop is introduced at z = 0 (injector face) subject to the initial conditions on its two velocity components and radius r_d and temperature T_d

$$u_d(0,\theta,t) = \text{constant} = u_d^\circ$$

$$v_d(0,\theta,t) = 0 = v_d^\circ$$

$$r_d(0,\theta,t) = \text{constant} = r_d^\circ \tag{6}$$

$$T_d(0,\theta,t) = \text{constant } T_d^\circ$$

The conditions given by system (6) form the set of initial conditions for the set of ordinary differential equations that couple to the set of partial differential equations (1). These equations are the momentum equations in the z and θ directions.

$$\frac{du_d}{dt} = \frac{u_d}{\partial t} + u_d \frac{\partial u_d}{\partial z} = \frac{1}{\rho_d} F_z$$

$$\frac{dv_d}{dt} = \frac{\partial v_d}{\partial t} + v_d \frac{\partial v_d}{\partial \theta} = \frac{1}{\rho_d} F_\theta \qquad (7)$$

and the mass and energy conservation equations for the drop

$$\frac{d\rho_d r_d^3}{dt} = - \frac{3}{4\pi} \dot{m}_d$$

$$\frac{dT_d}{dt} = q_d, \rho_d = \rho_d(T_d) \qquad (8)$$

The droplet density ρ_d is assumed to have a dependence only through the drop temperature T_d. The model of evaporation and combustion one chooses will determine the heat transfer to the drop q_d as well as the mass imigration $\dot{m}_d$ from the drop. Equations (7) are used to track the coordinates of the injected drops through the combustor. The tracking process ceases if

$$r_d < .1 r_d^\circ$$

since the mass associated with the drop would be less than one-thousandth the original injected value. All calculations presented in this report are with r_d° = 75 microns.

The evaporation and combustion process at any instant in time and space in the combustor is computed by finding the local drop parameters (by tracking each drop from its injection point) indicated by the right hand side of equations (7) and (8). If the drop does not exist at a mesh point, interpolation is used to determine r_d, T_d, u_d, and v_d at any arbitrary point (θ,z,t) in the interior of the combustor. For all computations presented the chamber length is

$0 \leq z \leq 2.1R$, R = 5.52 inches (chamber radius)

The combustors convergent-divergent nozzle is defined for values of z in

$2.1R < z \leq 3R$

The method of simulating a convergent-divergent nozzle in the annular chamber has been described in Reference 8.

The need of introducing the nozzle into the calculation is related to one's inability to describe the correct nonlinear time dependent downstream boundary conditions. The nozzle is a value that controls the pressure level in the combustor and hence the dependence of the outflow of combustion products from the combustor. One does not have to prescribe arbitrary conditions at the exit plane of the combustor. Rather, the flow is allowed to accelerate to a supersonic state within the nozzle and then the downstream boundary condition reduces to an extrapolation of flow conditions in the neighborhood of the supersonic boundary. The error introduced by this procedure, even though it can be made small, cannot propagate upstream into the chamber because the

particle speed exceeds the signal speed, i.e., signals are swept out of the domain of integration. It is felt that the methods used in determining the outflow conditions in the one-dimensional "annular" motors[2,6] be reexamined more critically. This is needed since the computation of the gradients of gas velocity, density and temperature in the z-direction in the plane z = constant require an assumption that introduces an integral condition over the entire domain of interest. This means that, if attention is directed to any arbitrary mesh point θ_i at time t, the dependence of the solution at θ_i at time $t+\Delta t$ depends not only on data at time t at mesh points θ_{i-1}, θ_i, θ_{i+1} (introduced from the difference quotients in the difference equation) but on all mesh values θ_i, i=1, 2, ..., J. This is seen from the integration formulas used (Simpson's Rule). Hence, at any time $t+\Delta t$ at point θ_i the solution depends on all other θ_k, k=1, 2, ..., J. The weights multiplying functions at each θ_k are uniform rather than decreasing as one moves away from the point θ_i. From fluid dynamic considerations this implies a violation of the rule of forbidden signals. Information at a point θ_p, where the distance

$$R(\theta_p-\theta_i)>(u+c)\Delta t,$$

can reach point θ_i in time Δt even though the inequality, as given above, is satisfied.

In fact, the stability condition

$$\frac{\Delta t}{R\Delta\theta} < \frac{1}{u+c}$$

is a necessary condition for stability for explicit schemes; here u and c are the particle velocity and sound speed respectively, $\Delta\theta = \theta_{i+1}-\theta_i$. For implicit methods this restriction may be relaxed, indeed the method may be unconditionally stable. However, even here, the dependence of the solution at a mesh point on neighboring mesh points will decrease with increasing mesh distance. This characteristic of difference methods is needed to model the behavior of the original differential equation.

III. NONSTEADY COMPUTATIONS

The conservation laws defining the combustion gas and the drops are integrated simultaneously[7,8,9] to define a steady state pressure, density and velocity field. In a previous report[9], we describe how to simulate a "pop" type of disturbance which is superimposed on the steady state. The first calculation presented shows the evolution of the disturbance in the annular motor where the sensitivity of the evaporation and combustion proess of the drop, a(p) is related to the pressure by

$$a(p) = \beta p^{.0108}$$

$$\beta = a(300)/300^{.0108}$$

$$a(300) = 3.73 \times 10^{-5}\ T + 1.855$$

The dimensionless burning rate at any pressure is a = a(p) while a(300) is the burning rate at 300 psia; it depends on the gas temperature. The mass evaporation of a droplet is proportional to a(p) - the exact relationship can be found in Reference (8). For the several computer runs presented in this report the dimensionless burning rate is taken to be

$$a(p;\lambda) = \beta p^{\lambda}$$

where λ is chosen for a particular run and $\beta = a(300)/300^{\lambda}$. We will present results for λ = 0.0108, 0.3 and 0.45.

The calculation is divided into two classes. One set, the first, shows the time dependent evolution of a simulated pulse or "pop" whose center is located at a point ($\theta = 270^{\circ}$, $z = 2$ inches). The maximum pressure of this pulse is 5810.7 psia; this pressure level corresponds to a dimensionless pressure of 19.4. The first set of figures conforms to a combustor with no baffles. The second set contains a baffle which is removed after the disturbance caused by the "pop" has moved around to the back of the baffle.

The baffle that has been introduced into the combustion chamber is called a shutter because it only exists in the chamber for a short time and allows the wave to be shaped and directed before it is removed. The shutter or removable baffle is placed at the line $\theta = \theta_j$ for $0 \leq z \leq L$, $L = 3.1R$. Conditions at the shutter from above are calculated by using the reflection values

$$\rho(z_i,\theta_{j-1},t_n) = \rho(z_i,\theta_{j+1},t_n)$$

$$u(z_i,\theta_{j-1},t_n) = u(z_i,\theta_{j+1},t_n) \qquad i=0,1,..I_L \quad n = 0,1,2,...$$

$$v(z_i,\theta_{j-1},t_n) = v(z_i,\theta_{j+1},t_n)$$

$$E(z_i,\theta_{j-1},t_n) = E(z_i,\theta_{j+1},t_n)$$

Conditions at the shutter from below are kept constant up to the point in time at which disturbances just reach the line $\theta = \theta_j$. This was done for ease of programming since the shutter is removed

before the wave coming around the chamber is sufficiently strong to greatly affect conditions below the shutter. Thus, the shutter is programmed by saving the values on the two lines below the shutter ($\theta=\theta_{j-1}$, $\theta=\theta_{j-2}$) at the beginning of each step. The values on the line below the shutter $\theta=\theta_{j-1}$, are then set to the reflection values and the program proceeds. At the end of the step the data on the line $\theta=\theta_{j-1}$ is set back to its original values. Since the line $\theta=\theta_{j-2}$ is affected by $\theta=\theta_{j-1}$, it is also similarly kept constant.

IV. RESULTS

Figures 1-14 show selected instants of time for the evolution of a "pop" in the annular combustor. The value of λ=0.0108 is used in this calculation. There is no baffle in this combustor. Figures 1 and 2 show the initial pressure field and velocity field. There are no contour lines showing the steady state pressure distribution in the chamber because the values of chamber pressure all lie between the contour levels 1 and 2. The large velocity increase indicates the position of the combustion nozzle. In Figure 3 we pick up the first contour line (2) in the combustor that corresponds to a steady state pressure value. The "pop" remains symmetric and moves towards the nozzle more rapidly than it is sweeping across the injector face.

Figure 4 is the velocity field corresponding to this pressure field. The velocities generated by the "pop" are as large as those that are in the nozzle. In looking at the following figures it is interesting to note the formation of another line of symmetry at $\theta=90^{\circ}$ where, as shown in Figure 10, a large value of pressure is produced due to the collision of the two symmetric disturbances generated by the "pop". Two more waves are produced which move away from each other (Figure 10). Figures 12-15 show how quickly the combustor is moving towards its original steady state value.

Figure 16 is, in one sense, a complete record of this calculation. It shows the maximum and minimum pressure in the combustor at each instant of time. In addition, the pressure histories (p(t))

at 3 locations in the chamber are shown. Due to scaling problems (at the time this plot was generated) the initial transient of the "pop" has been deleted. It is shown in other figures which were generated more recently. However, the interesting feature of this graph is that the maximum peak to peak variation in the maximum pressure is ($t>0.60$ millisec) of the order of 25 psia while local pressure oscillations are much larger ($p(3)$). This would indicate that maximum peak to peak measurements of maximum chamber pressure may only be indicative of much larger transient motions existing in the combustion chamber.

Figures 17 to 30 are the snapshots of the time dependent solution of a shuttered chamber with $\lambda=0.45$. The initial conditions for this case are shown in Figures 1 and 2. Note the absence of a second line of symmetry as in the previous calculations. Figure 19 may be compared with Figure 5 to see the effect of the baffle on the flow field. The printouts of each of these cases are approximately at the same physical time and may be compared.

Figures 31 and 32 are the complete time history for the pressure in the combustor for $\lambda=.0108$. Figure 32 is a repeat of Figure 16. This set of figures may be compared to Figures 33 and 34 for the same value of λ but with a baffle located in the engine for the latter figures. There does not appear to be a great difference between these two cases.

Figures 35-36 and 37-38 are shuttered calculations with λ=0.30 and λ=0.45 respectively. The greatest difference appears in the larger oscillations in the variation in the peak to peak pressure of the maximum pressure trace as λ gets larger and larger. The location of the individual traces are given by the coordinates on the graph (p_1 is located at θ=270°, z=? inches from the injector). The position chosen was arbitrary and will, for future runs, coincide with the pressure taps of the JPL annular engine.

Our conclusions on the calculations that have as far been completed are mixed. We feel we have a code that successfully couples a droplet spray to a nonlinear gas dynamic environment. We can successfully pulse this environment with rather large amplitude waves. We have as yet not succeeded in producing a wave that will reside in the chamber and spin in the neighborhood of the injector for a reasonably long time. We do, however, see a dependence of wave amplitude on intensity (λ) of combustion as measured by peak to peak pressure amplitudes.

V. BOUNDARY CONDITIONS

Dependence of the solution for the pancake motor (computer code COMB) on the boundary condition at the chamber wall is shown in the next few figures. We have chosen the code COMB to shed some light on the effect of choosing boundary conditions for the difference equations. The boundary condition for the differential equation is

$$u(r,0,t) = 0 \text{ at } r = R$$

The difference equations, however, need data (on r = R) in excess of the above single condition. Since we are solving a system of four difference equations in four unknowns, an additional three conditions are required for the set of difference equations being used.

The guide taken can come from characteristic methods; however, for shocked flows, that method, based on differentiability of the solution, may lead to errors at the boundary.

The technique used to generate the results shown here is motivated by looking at the momentum equation in the normal direction to the wall - the radial momentum equation if the normal velocity at the wall is initially zero, then we wish to state conditions on ρ, v and p which will assure that the time derivative of u at the wall will also be zero. If D_o represents the centered difference, then choosing

$$D_o p = \frac{\rho v^2}{R} h$$

$$D_o v = 0$$

$$D_o u = 2uh$$

$$D_o \rho' = 0$$

in which $h = \Delta r$ and $\rho' = \rho r$ and the terms on the right hand side are defined at mesh points $(r-h,\theta,t)$, the forward time difference will attain the value

$$\frac{u(t+\Delta t)-u(t)}{\Delta t} = 0 \ .$$

In order to test these conditions we chose a problem in which an exact solution is available. The problem of the first spinning mode in a circular chamber obtained by solving the linear wave equation subject to the condition $u(r,\theta,t) = 0$ on the boundary is available in closed form and may be compared to two nonlinear finite difference calculations. The first solution is obtained using the boundary conditions just given, the second is changed only in one way - using a modified pressure extrapolation: $D_o p=0$. If the amplitude (ϵ) of the first spinning mode for the numerical calculation is taken to be small, there is no difference in the solution for the two techniques used. Also, they both agree with the exact solution to at least six decimal places. The reason

that both numerical solutions agree is that the term $\rho v^2/R$ is quite small - of the order ε^2. Hence, the value of $D_o p = (h\varepsilon^2)$.

A relatively large value of ε must be chosen to observe any difference between the two numerical solutions. For the value of ε, chosen the numerical calculation shows that there are nonlinear effects already present. Hence, there is only approximate agreement between the "exact linear solution" and the numerical solutions. The most important difference between the two numerical solutions is the oscillation at the boundary of the solution that uses the modified extrapolated value of the pressure gradient. On the other hand, the numerical solution subject to the original boundary conditions remain smooth. If the amplitude ε is allowed to increase further, the solution corresponding to the modified boundary condition goes unstable as the oscillations from the boundary eventually swamp the solution in the interior. The boundary conditions leading to a smooth solution are reflection rules modified to take the polar coordinate system into account. Figure 39 is the exact linear solution at 91/100 of the first revolution while Figure 40 is the numerical solution obtained using the reflection rules. Figure 41 is the elliptic streakline generated by this numerical solution. Finally, Figure 42 is the pressure field generated by the numerical solution using the boundary condition $D_o p = 0$.

VI. CONCLUSIONS

A model of a two-dimensional annular combustion chamber has been programmed for a digital computer. A droplet model in two dimensions is coupled to the gas dynamics so that interactions of arbitrary nature can occur, i.e., the relative velocity between the droplets and the gas will depend on the local conditions. No assumption on the rate of gas flow leaving the combustion zone is required. The pressure oscillation levels which can be considered and have been computed are of the order of 20 when expressed as a ratio of the steady state pressure.

It is felt that the present model is mathematically more realistic than previous one-dimensional models insofar as the boundary conditions on the gas dynamic flow is correctly stated. Most important, however, although measured peak to peak pressure oscillations in our computations surpass those reported in the literature, it is still not clear at this writing if instability of the type reported by Clayton[10] has actually been observed. Since computer experiments have just started with this model, it is too early to come to definite conclusions about stability of combustion based on an evaporation rate controlled model.

1. Priem, R. J. and Heidmann, M. F., "Propellant Vaporization as a Design Criterion for Rocket-Engine Combustion Chambers", NASA TR R-67, 1960.

2. Priem, R. J. and Gruentert, D. C., "Combustion Instability Limits Determined by a Nonlinear Theory and a One-Dimensional Model", NASA TN D-1409, 1962.

3. Clayton, R. M. and Rogero, R. S., "Experimental Measurements on a Rotating Detonation-like Wave Observed During Liquid Rocket Resonant Combustion", J.P.L. TR No. 32-788, August 15, 1965.

4. Crocco, L. and Cheng, S. I., "Theory of Combustion Instability in Liquid Propellant Rocket Motors", AGARD Monograph No. 8, Butterworths Scientific Publications, Ltd., London, 1956.

5. Crocco, L., Greg, J. and Harrje, D. T., "Theory of Liquid Propellant Rocket Combustion Instability and its Experimental Verification", ARS Journal, Vol. 30, No. 2, Feb. 1960.

6. Campbell, D. T. and Chadwick, W. D., "Combustion Instability Analysis at High Chamber Pressure", Final Report, AFRPL-TR-68-179, Rocketdyne August, 1968.

7. Burstein, S. Z., "Nonlinear Combustion Instability in Liquid-Propellant Rocket Engines: The Transverse Mode 1. The Hydrodynamic Differential and Difference Equations and Computer Algorithm", NASA TR 32-1111, Sept. 15, 1967.

8. Burstein, S. Z., Chinitz, W., and Schechter, H., "Nonlinear Combustion Instability in Liquid-Propellant Rocket Motors", MAGI Final Report to J.P.L., Contract No. 951946, June, 1969.

9. Burstein, S. Z., and Schechter, H., "Nonlinear Combustion Instability: Computer Experiments Using Codes COMB and TRDL", MAGI Final Report of J.P.L., Contract No. 952505, July, 1969.

10. Clayton, R. M., "Resonant Combustion", J.P.L. Space Programs Summary 37-55, Vol. 3, February 28, 1969.

KUSHIDA POP ENERGY

PRESSURE ISOBARS

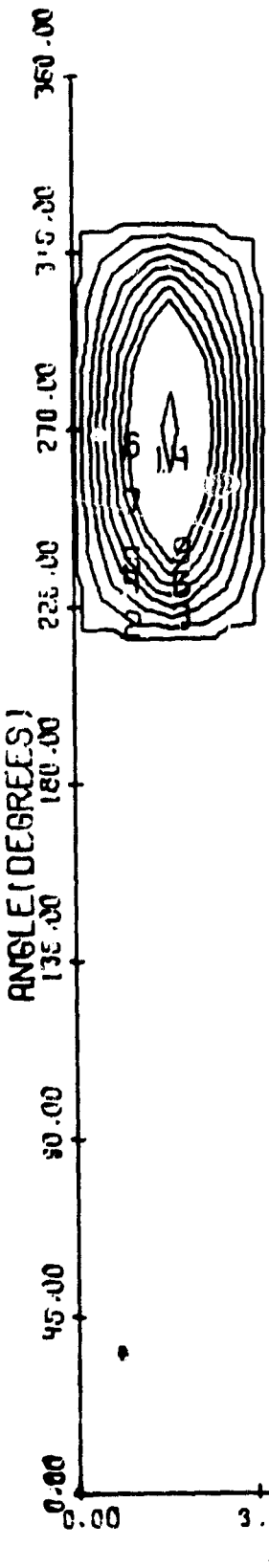

T= 0.000 MILLISECONDS

ISOBAR	PRESSURE(PSI)
1	25.154
2	438.404
3	851.654
4	1264.904
5	1678.154
6	2091.404
7	2504.654
8	2917.904
9	3331.154
10	3744.405
11	4157.655
12	4570.905
13	4984.155
14	5397.405
15	5810.655

PREF=REFERENCE PRESSURE = 300.00 PSI
AREF=REFERENCE SOUND SPEED= 3220.7 FT/SEC
R =CHAMBER RADIUS = .45830 FEET
TREF=REFERENCE TIME=R/AREF=.0001423 SEC

T/TREF= 0.00000

ISOBAR	PRESSURE/PREF
1	.084
2	1.461
3	2.839
4	4.216
5	5.594
6	6.971
7	8.349
8	9.726
9	11.104
10	12.481
11	13.859
12	15.236
13	16.614
14	17.991
15	19.369

FIG. 1

T= 0.000 MILLISECONDS

KUSHIDA POP ENERGY

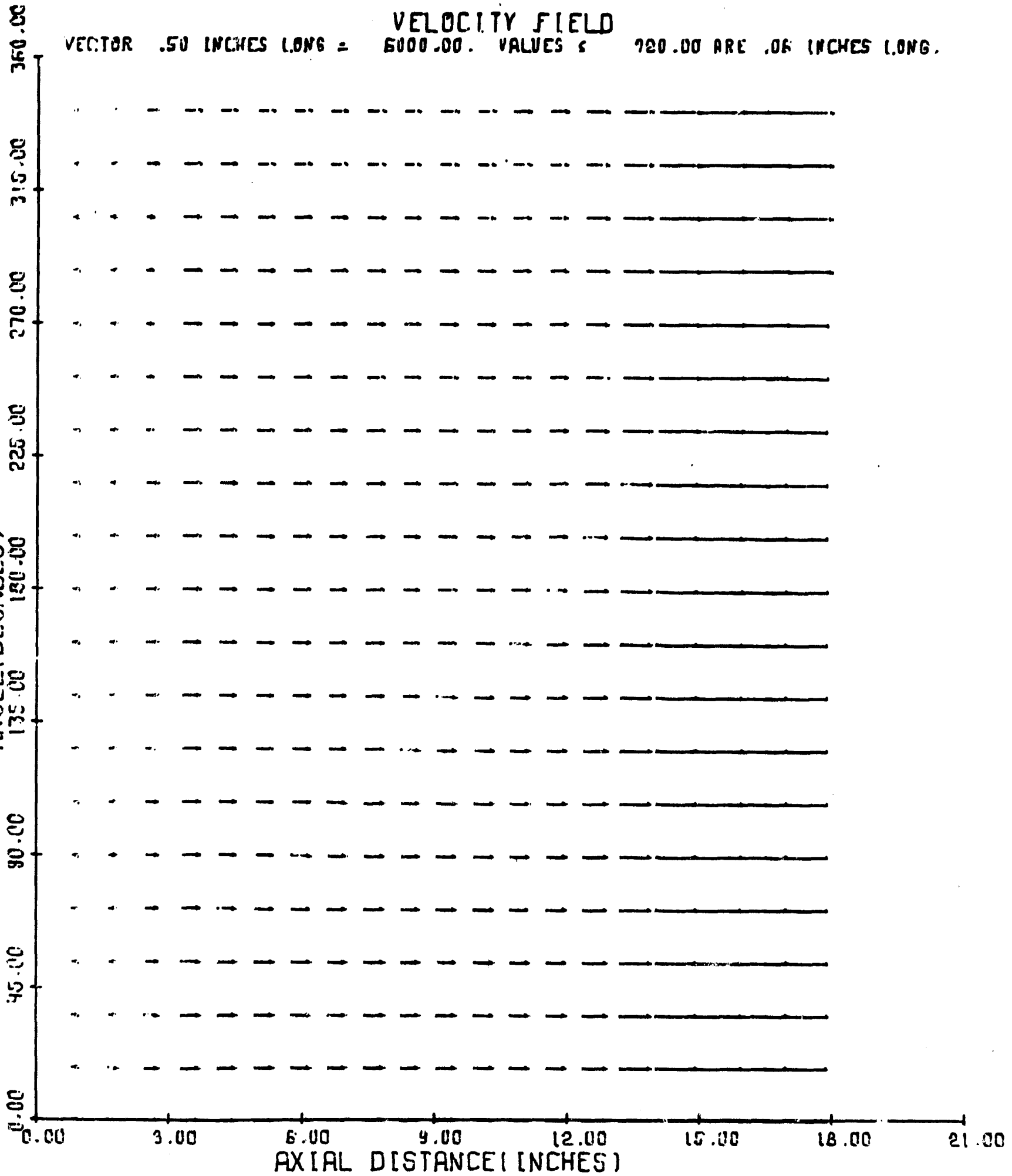

FIG. 2

T= 0.000 MILLISECONDS

KUSHIDA POP ENERGY

PRESSURE ISOBARS

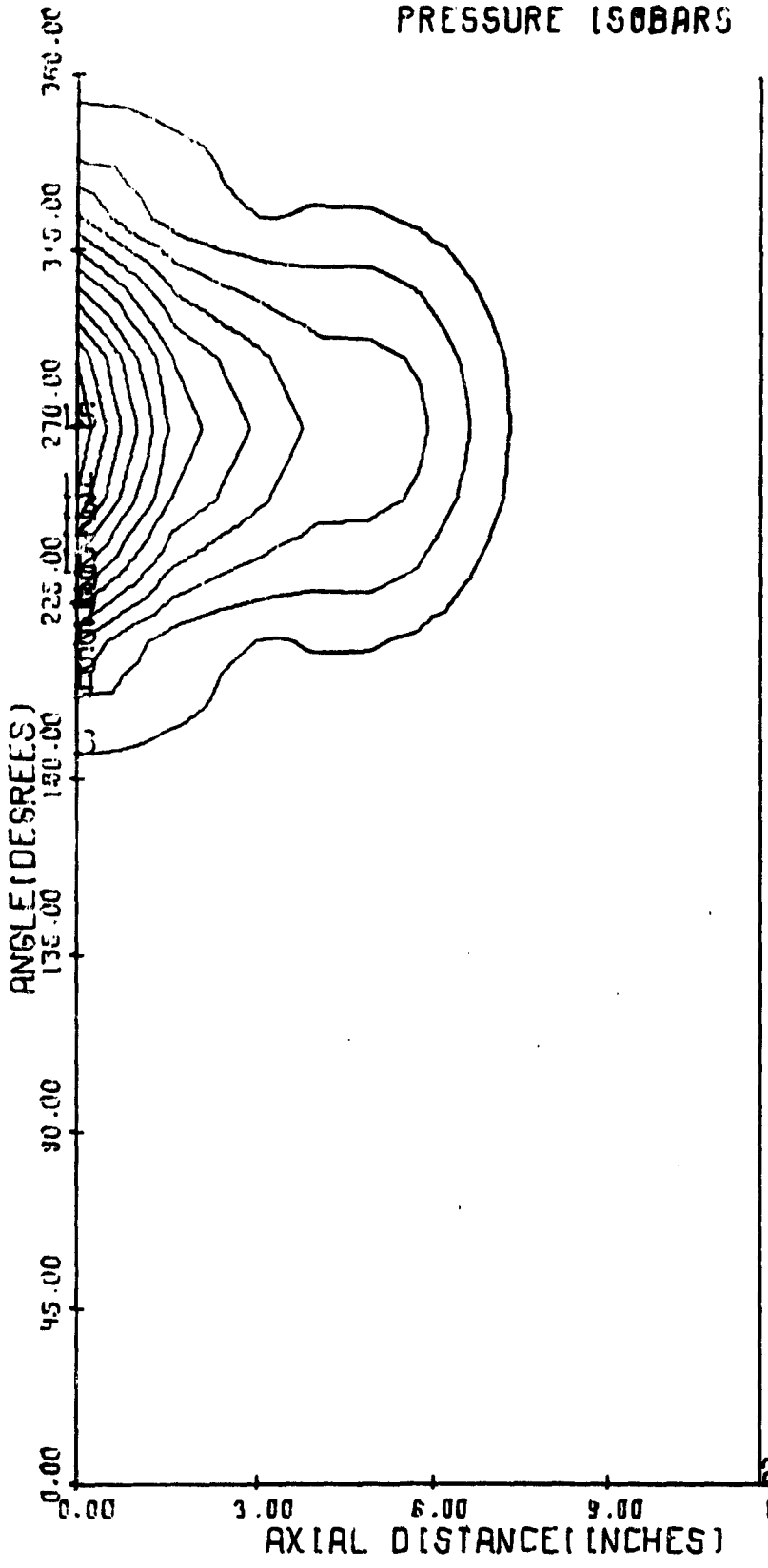

T= .048 MILLISECONDS

T= .048 MILLISECONDS

ISOBAR	PRESSURE(PSI)
1	48.486
2	222.965
3	397.444
4	571.923
5	746.403
6	920.882
7	1095.361
8	1269.840
9	1444.319
10	1618.798
11	1793.278
12	1967.757
13	2142.236
14	2316.715
15	2491.194

PREF=REFERENCE PRESSURE = 360.00 PSI
AREF=REFERENCE SOUND SPEED= 3220.7 FT/SEC
R =CHAMBER RADIUS = .45830 FEET
TREF=REFERENCE TIME=R/AREF=.0001423 SEC

T/TREF= .33916

ISOBAR	PRESSURE/PREF
1	.162
2	.743
3	1.325
4	1.906
5	2.488
6	3.070
7	3.651
8	4.233
9	4.814
10	5.396
11	5.978
12	6.559
13	7.141
14	7.722
15	8.304

FIG. 3

KUSHIDA POP ENERGY

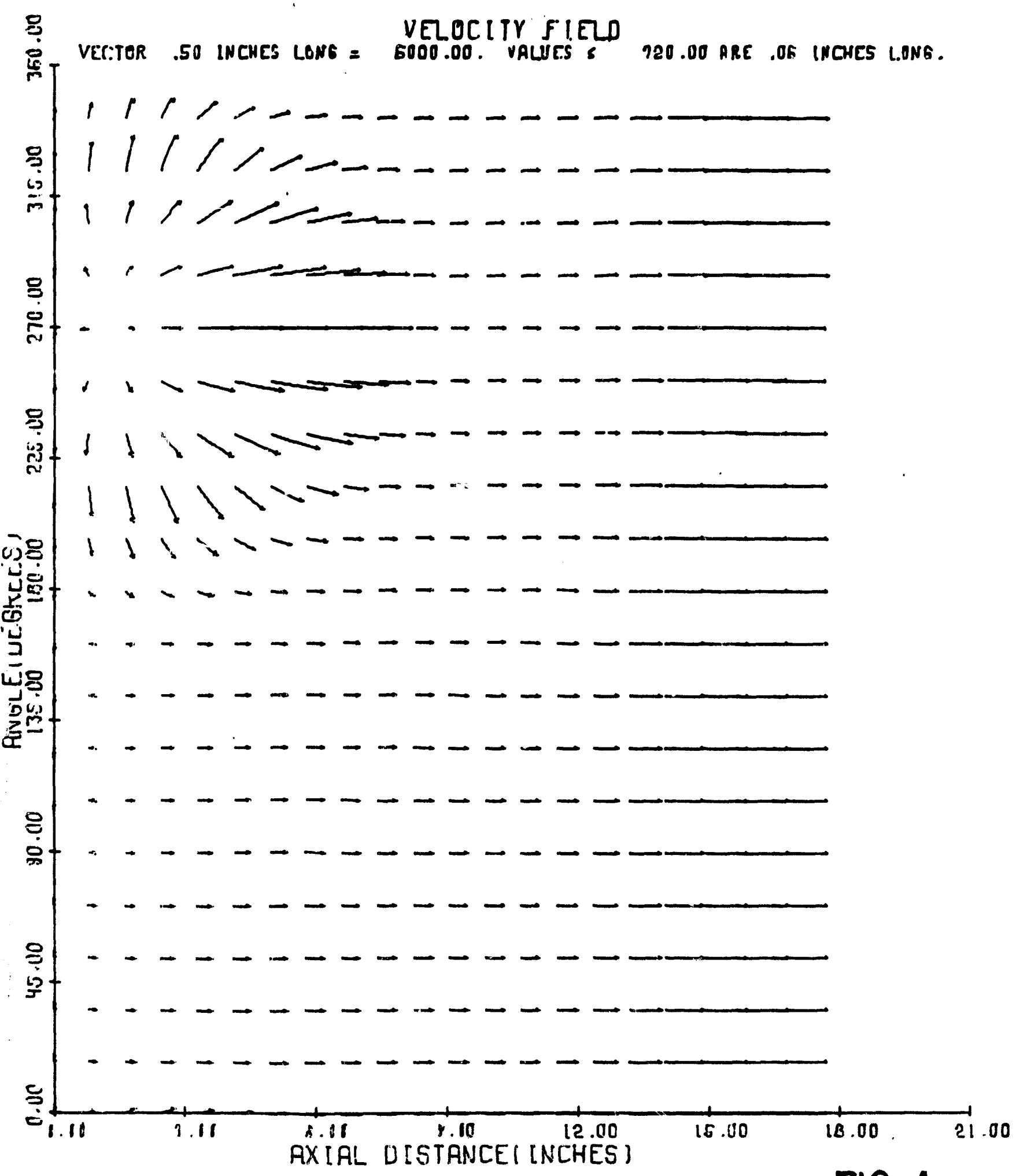

FIG. 4

T= .048 MILLISECONDS

KUSHIDA POP ENERGY

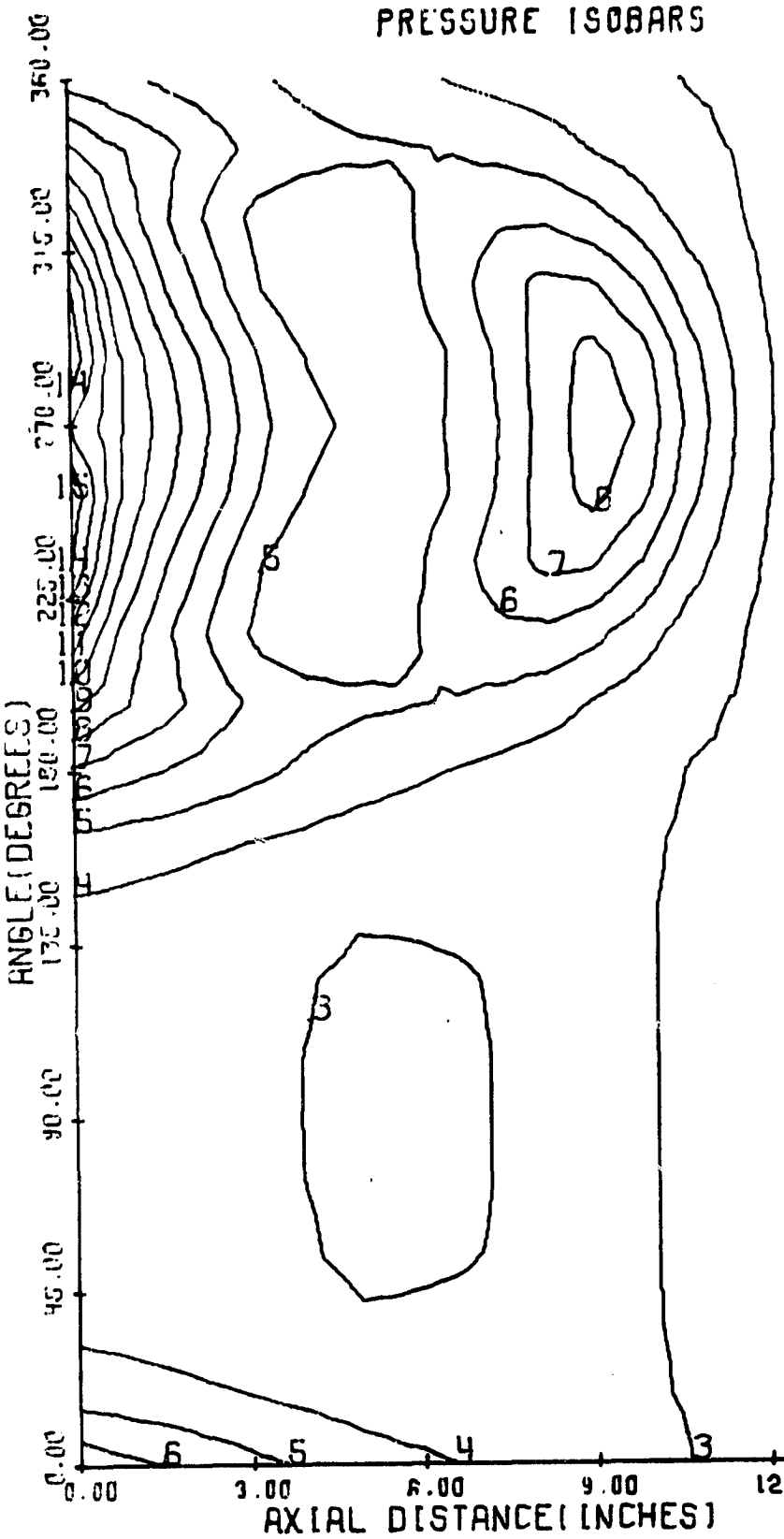

T= .094 MILLISECONDS

ISOBAR	PRESSURE(PSI)
1	59.586
2	143.190
3	226.793
4	310.396
5	394.000
6	477.603
7	561.206
8	644.810
9	728.413
10	812.016
11	895.620
12	979.223
13	1062.826
14	1146.430
15	1230.033

PREF=REFERENCE PRESSURE = 300.00 PSI
AREF=REFERENCE SOUND SPEED= 3220.7 FT/SEC
R =CHAMBER RADIUS = .45830 FEET
TREF=REFERENCE TIME=R/AREF=.0001423 SEC

T/TREF= .66147

ISOBAR	PRESSURF/PREF
1	.199
2	.477
3	.756
4	1.035
5	1.313
6	1.592
7	1.871
8	2.149
9	2.428
10	2.707
11	2.985
12	3.264
13	3.543
14	3.821
15	4.100

FIG.5

T= .094 MILLISECONDS

KUSHIDA POP ENERGY

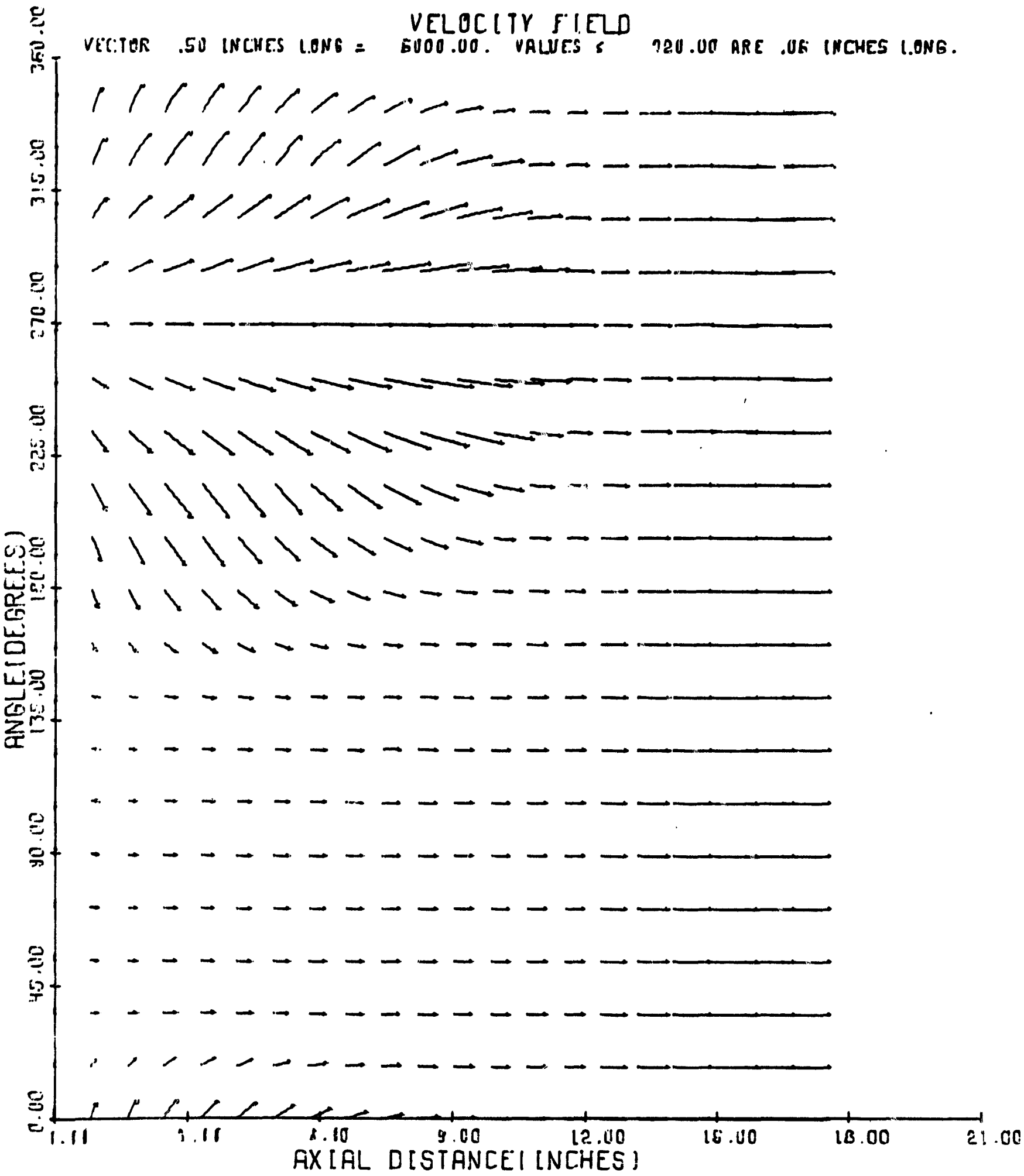

FIG. 6

T= .094 MILLISECONDS

KUSHIDA POP ENERGY

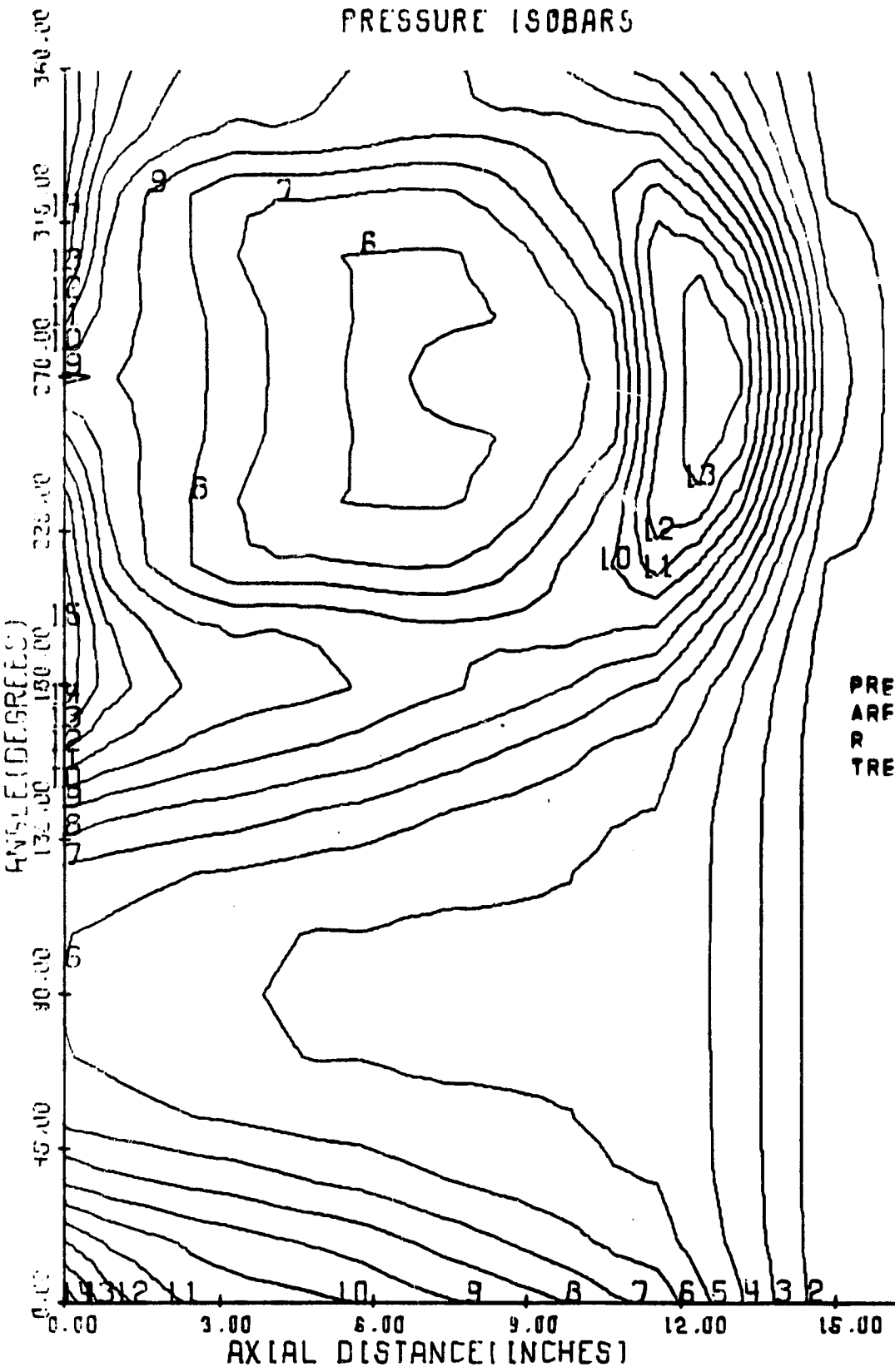

T= .141 MILLISECONDS

ISOBAR	PRESSURE(PSI)
1	49.747
2	93.192
3	136.636
4	180.080
5	223.525
6	266.969
7	310.414
8	353.858
9	397.303
10	440.747
11	484.192
12	527.636
13	571.080
14	614.525
15	657.969

PREF=REFERENCE PRESSURE = 300.00 PSI
AREF=REFERENCE SOUND SPEED= 3220.7 FT/S
R =CHAMBER RADIUS = .45830 FEET
TREF=REFERENCE TIME=R/AREF=.0001423 SEC

T/TREF= .99364

ISOBAR	PRESSURE/PREF
1	.166
2	.311
3	.455
4	.600
5	.745
6	.890
7	1.035
8	1.180
9	1.324
10	1.469
11	1.614
12	1.759
13	1.904
14	2.048
15	2.193

FIG. 7

T= .141 MILLISECONDS

KUSHIDA POP ENERGY

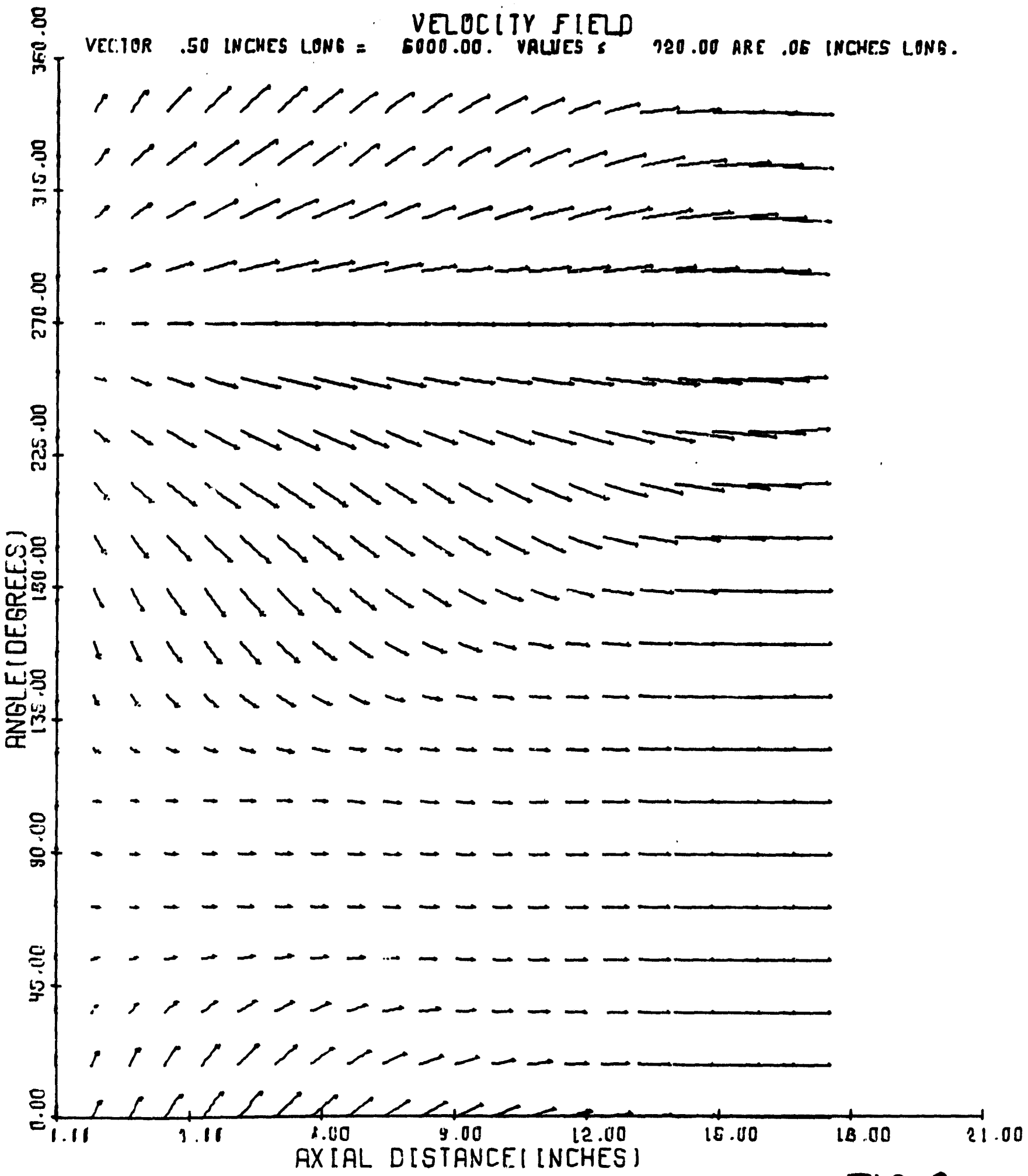

FIG. 8

T= .141 MILLISECONDS

KUSHIDA POP ENERGY

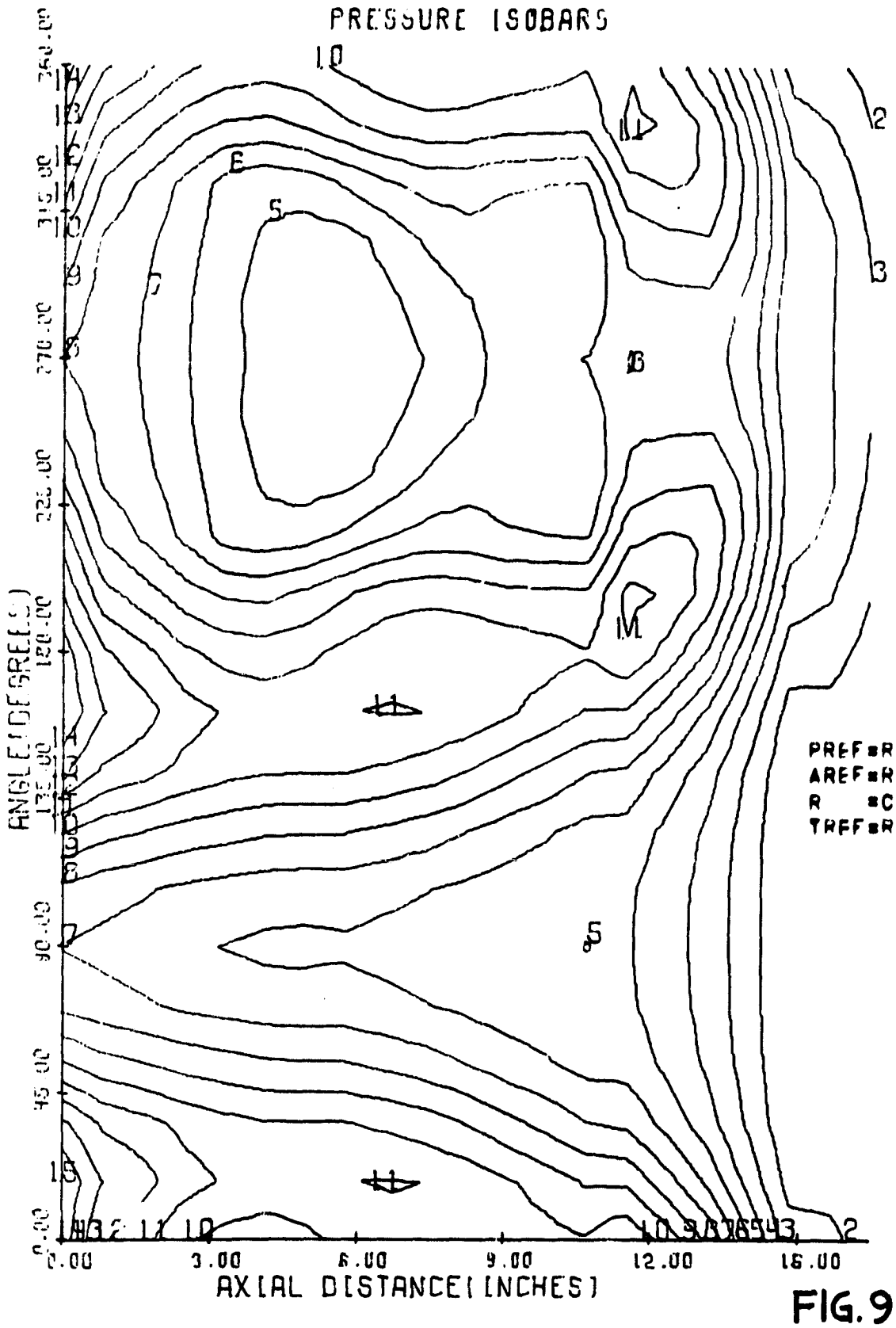

FIG. 9

T= .182 MILLISECONDS

T= .182 MILLISECONDS

ISOBAR	PRESSURE(PSI)
1	62.206
2	98.082
3	133.957
4	169.832
5	205.708
6	241.583
7	277.458
8	313.334
9	349.209
10	385.085
11	420.960
12	456.835
13	492.711
14	528.586
15	564.461

PREF=REFERENCE PRESSURE = 300.00 PSI
AREF=REFERENCE SOUND SPEED= 3220.7 FT/SE
R =CHAMBER RADIUS = .45830 FEET
TREF=REFERENCE TIME=R/AREF=.0001423 SEC

T/TREF= 2.23921

ISOBAR	PRESSURE/PREF
1	.097
2	.236
3	.375
4	.514
5	.653
6	.792
7	.931
8	1.070
9	1.209
10	1.348
11	1.487
12	1.626
13	1.765
14	1.905
15	2.044

KUSHIDA POF ENERGY

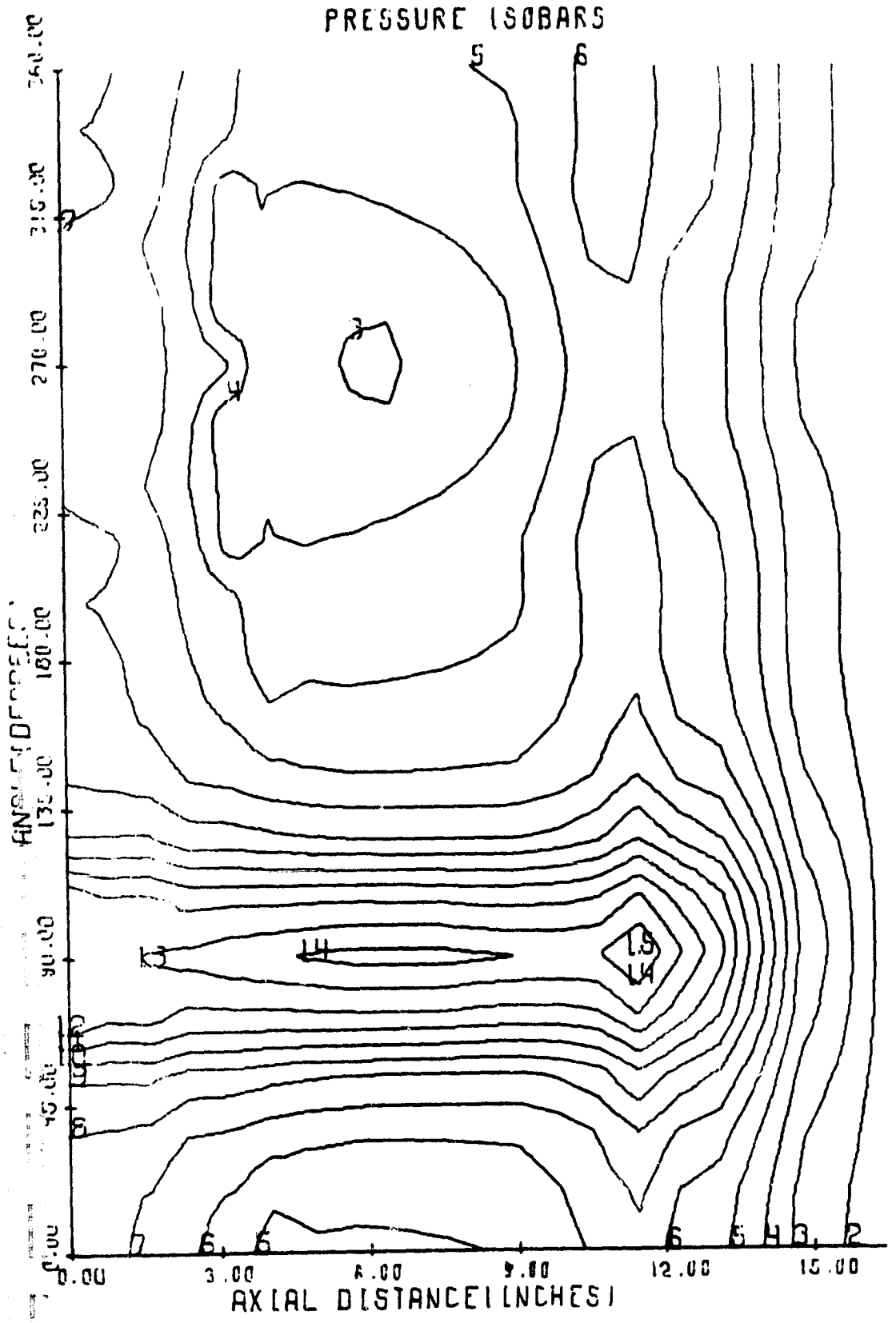

T= .319 MILLISECONDS

T= .319 MILLISECONDS

ISOBAR	PRESSURE (PSI)
1	29.041
2	70.758
3	112.474
4	154.191
5	195.907
6	237.624
7	279.340
8	321.057
9	362.773
10	404.490
11	446.206
12	487.923
13	529.639
14	571.356
15	613.072

PREF=REFERENCE PRESSURE = 300.00 PSI
AREF=REFERENCE SOUND SPEED= 3220.7 FT/SEC
R =CHAMBER RADIUS = .45830 FEET
TREF=REFERENCE TIME=R/AREF=.0001423 SEC

T/TREF= 1.27758

ISOBAR	PRESSURE/PREF
1	.207
2	.327
3	.447
4	.566
5	.686
6	.805
7	.925
8	1.044
9	1.164
10	1.284
11	1.403
12	1.523
13	1.642
14	1.762
15	1.882

FIG. 10

KUSHIDA POP ENERGY

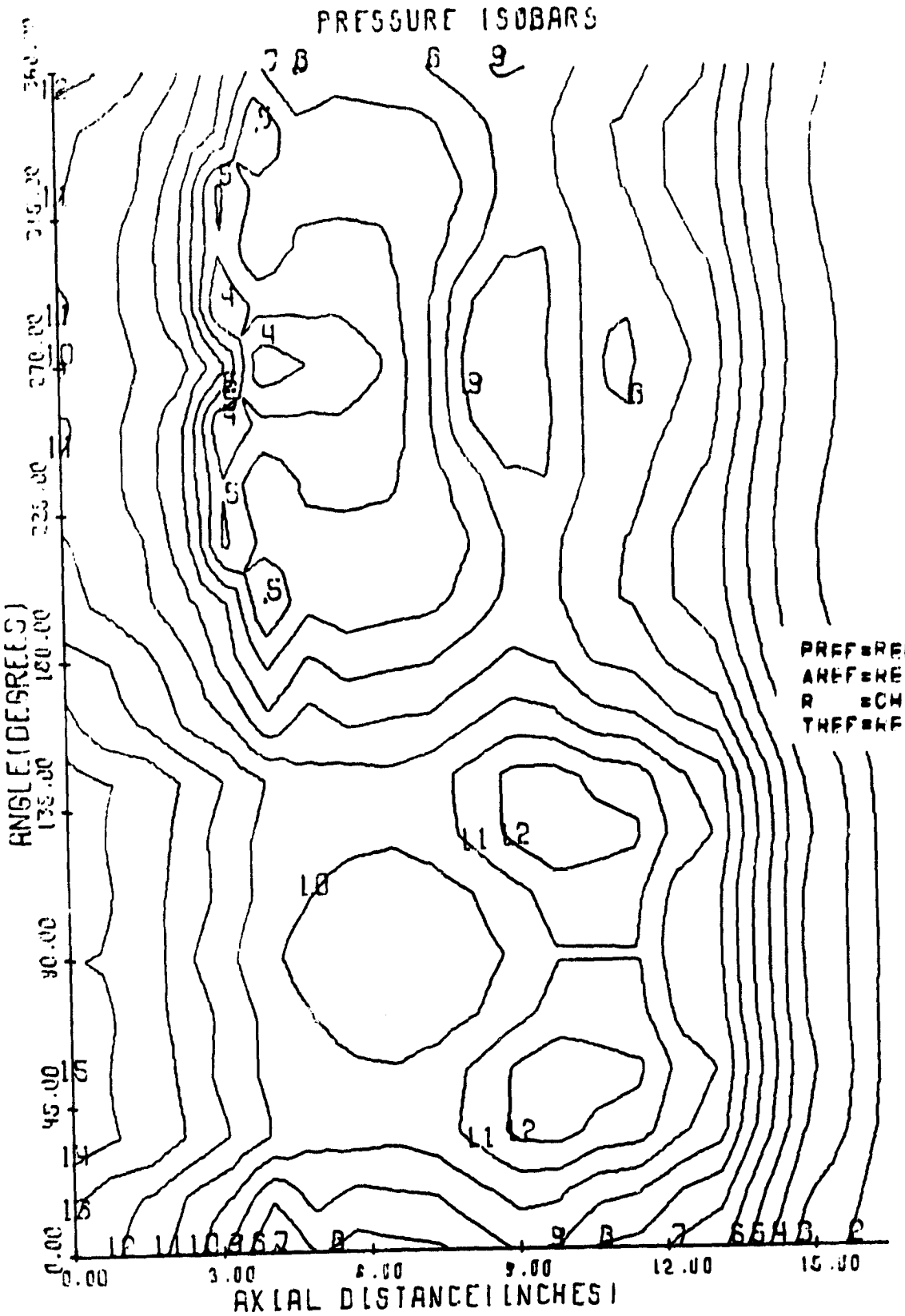

T= .462 MILLISECONDS

ISOBAR	PRESSURE(PSI)
1	19.465
2	48.600
3	77.735
4	106.870
5	136.005
6	165.140
7	194.276
8	223.411
9	252.546
10	281.681
11	310.816
12	339.951
13	369.087
14	398.222
15	427.357

PREF=REFERENCE PRESSURE = 300.00 PSI
AREF=REFERENCE SOUND SPEED= 3220.7 FT/SEC
R =CHAMBER RADIUS = .45830 FEET
TREF=REFERENCE TIME=R/AREF=.0001423 SEC

T/TREF= 3.24341

ISOBAR	PRESSURE/PREF
1	.065
2	.162
3	.259
4	.356
5	.453
6	.550
7	.648
8	.745
9	.842
10	.939
11	1.036
12	1.133
13	1.230
14	1.327
15	1.425

30

FIG. 11

KUSHIDA POP ENERGY

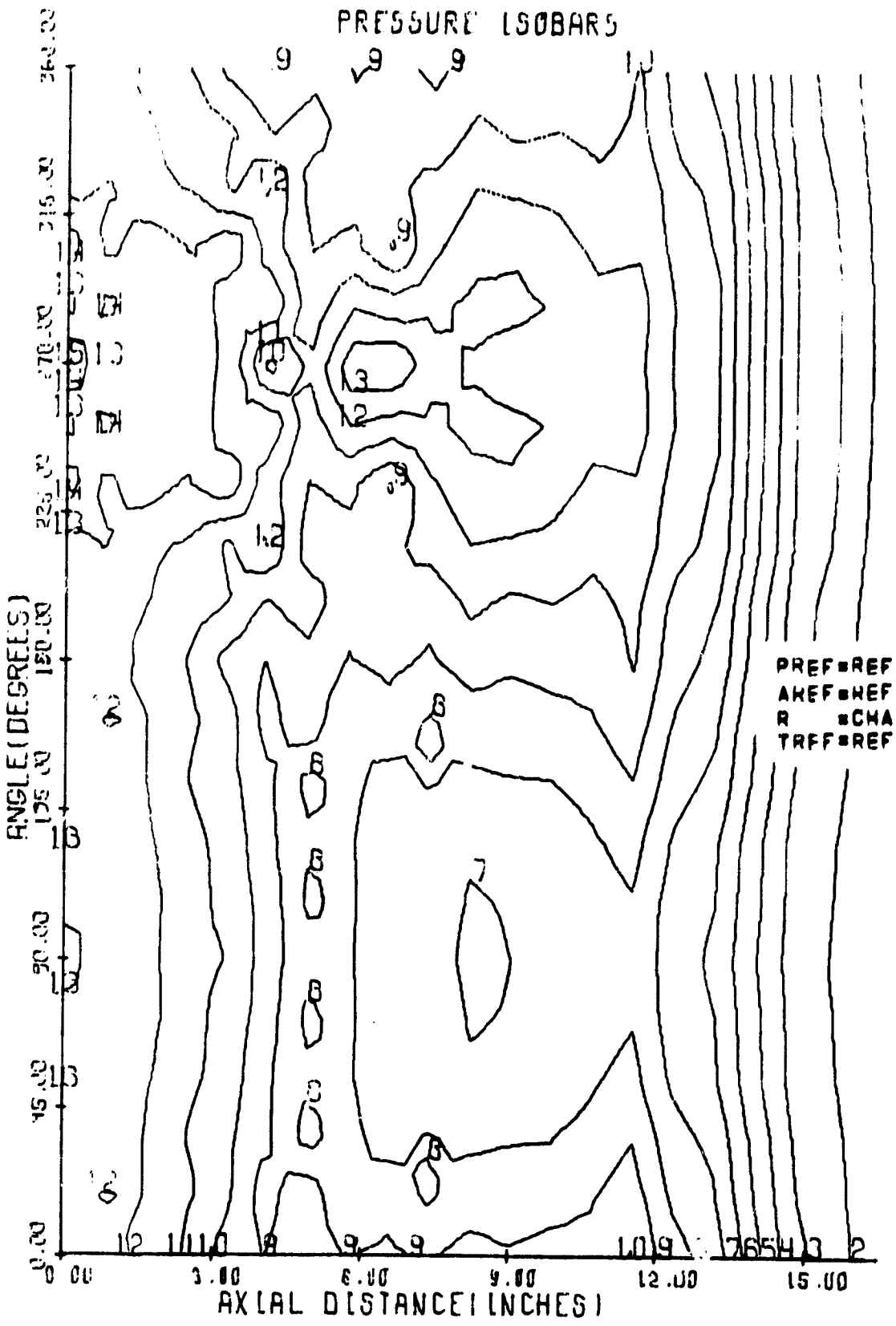

T= .862 MILLISECONDS

ISOBAR	PRESSURE(PSI)
1	19.665
2	46.330
3	72.995
4	99.660
5	126.325
6	152.990
7	179.655
8	206.321
9	232.986
10	259.651
11	286.316
12	312.981
13	339.646
14	366.311
15	392.976

PREF=REFERENCE PRESSURE = 300.00 PSI
AREF=REFERENCE SOUND SPEED= 3220.7 FT/SEC
R =CHAMBER RADIUS = .45810 FEET
TREF=REFERENCE TIME=R/AREF=.0001423 SEC

T/TREF= 6.05451

ISOBAR	PRESSURE/PREF
1	.066
2	.154
3	.243
4	.332
5	.421
6	.510
7	.599
8	.688
9	.777
10	.866
11	.954
12	1.043
13	1.132
14	1.221
15	1.310

FIG. 12

T= .862 MILLISECONDS

KUSHIDA POP ENERGY

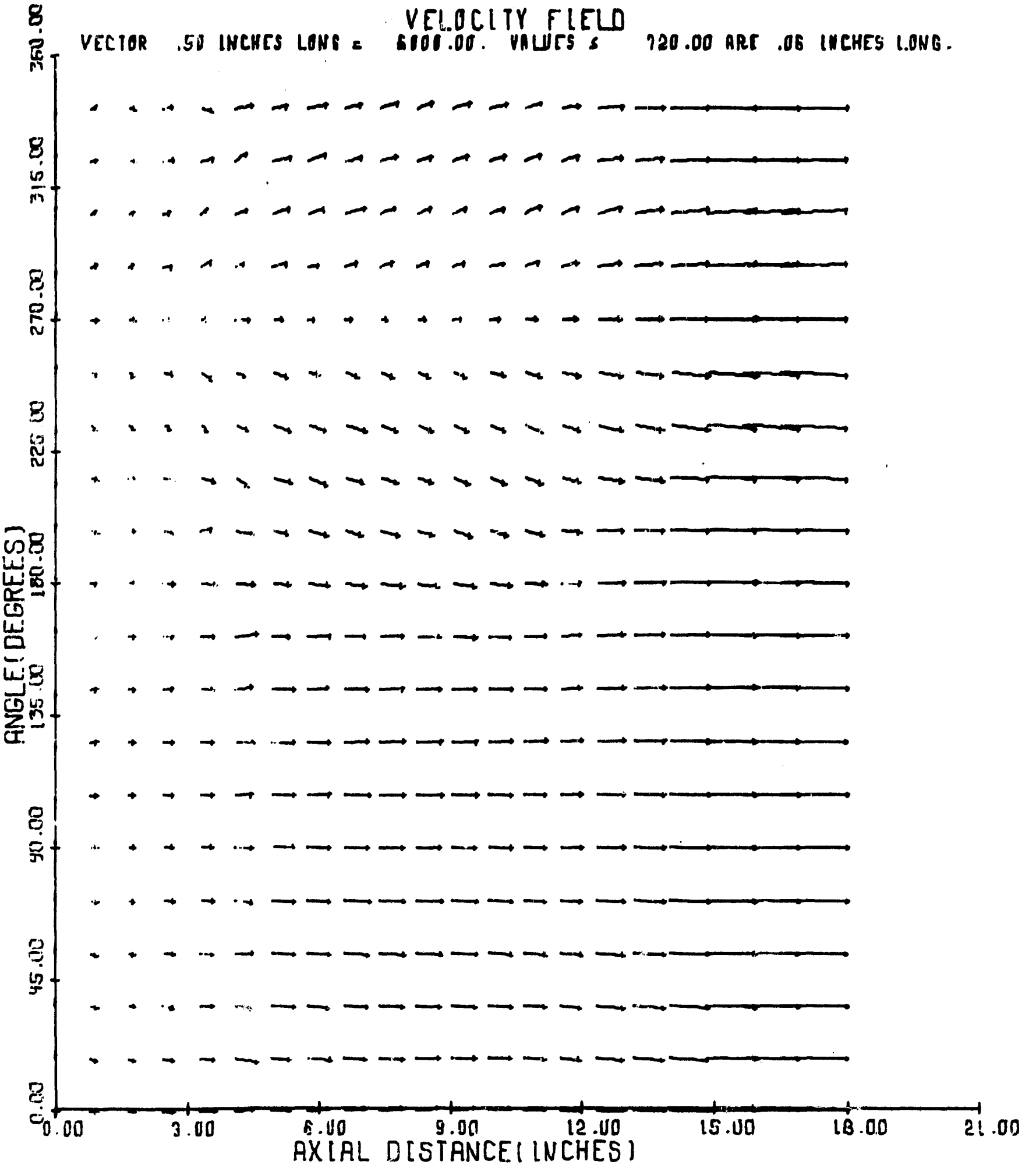

FIG. 13

T= .862 MILLISECONDS

KUSHIDA POP ENERGY

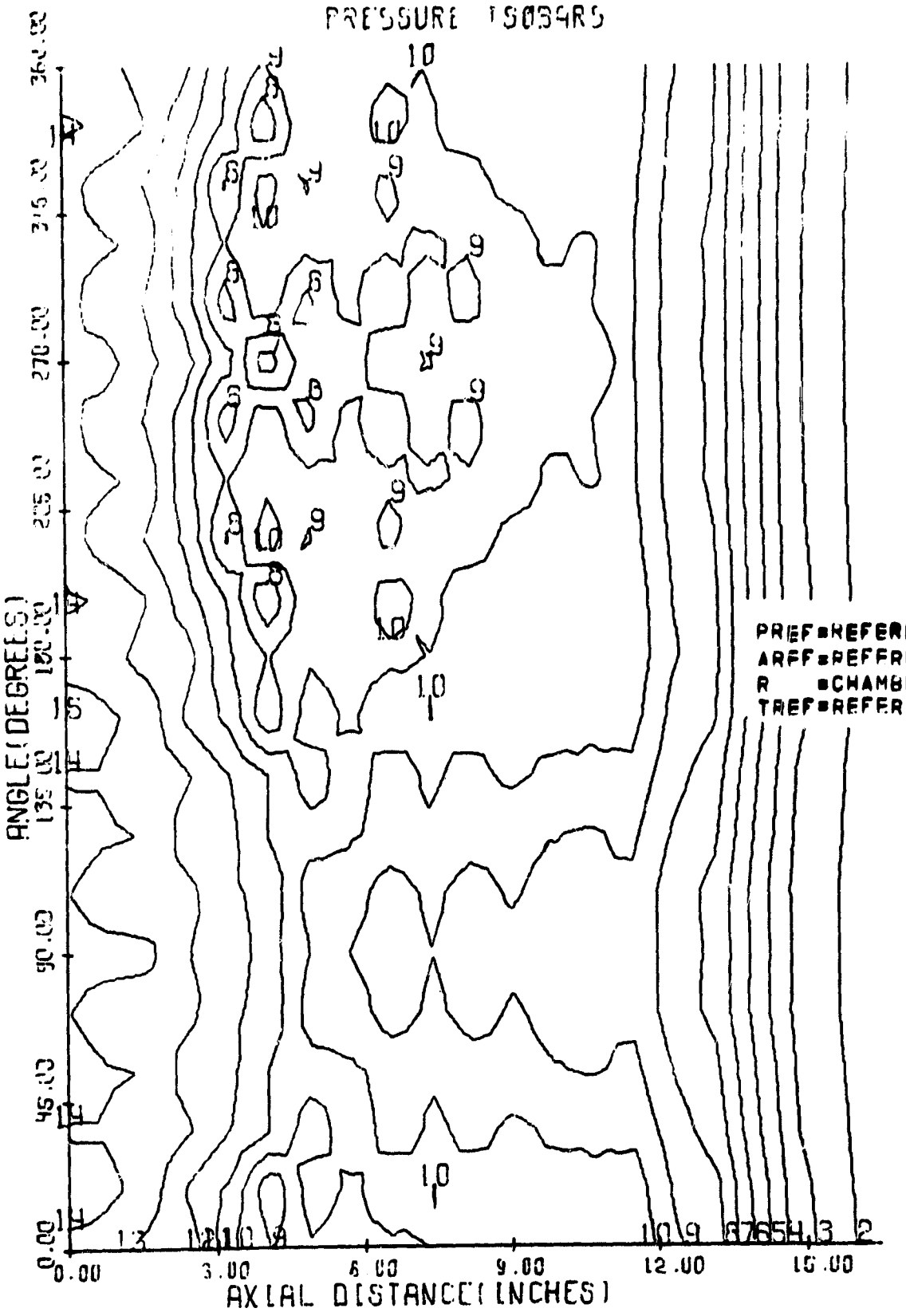

T= 1.476 MILLISECONDS

ISOBAR	PRESSURE(PSI)
1	25.446
2	51.334
3	77.222
4	103.110
5	128.998
6	154.886
7	180.774
8	206.662
9	232.550
10	258.438
11	284.326
12	310.214
13	336.102
14	361.990
15	387.878

PREF=REFERENCE PRESSURE = 300.00 PSI
AREF=REFERENCE SOUND SPEED= 3220.7 FT/SEC
R =CHAMBER RADIUS = .45830 FEET
TREF=REFERENCE TIME=R/AREF=.0001423 SEC

T/TREF= 10.37526

ISOBAR	PRESSURE/PREF
1	.085
2	.171
3	.257
4	.344
5	.430
6	.516
7	.603
8	.689
9	.775
10	.861
11	.948
12	1.034
13	1.120
14	1.207
15	1.293

FIG. 14

T= 1.476 MILLISECONDS

KUSHIDA POP ENERGY

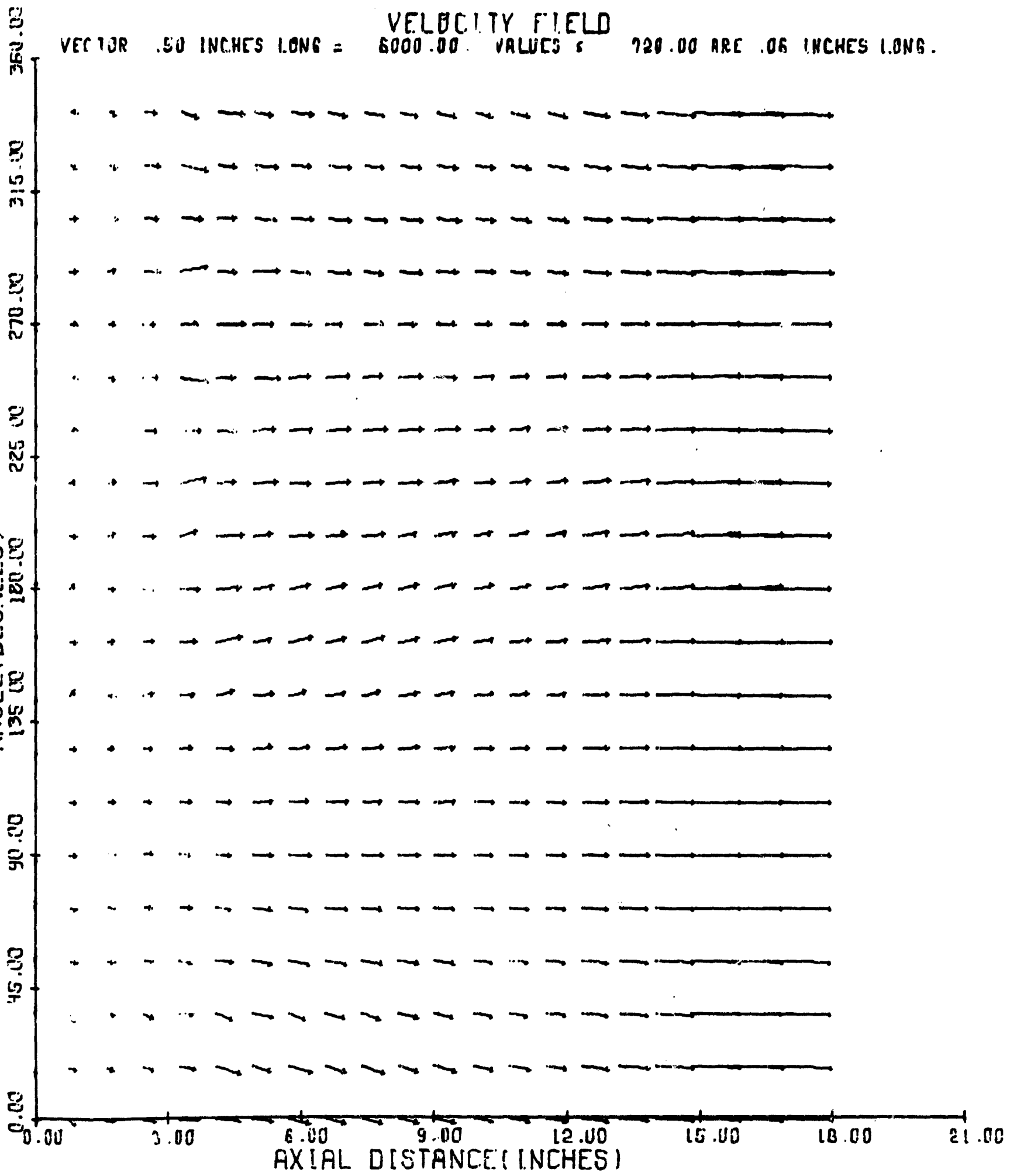

FIG. 15

T= 1.476 MILLISECONDS

KUSHIDA POP ENERGY

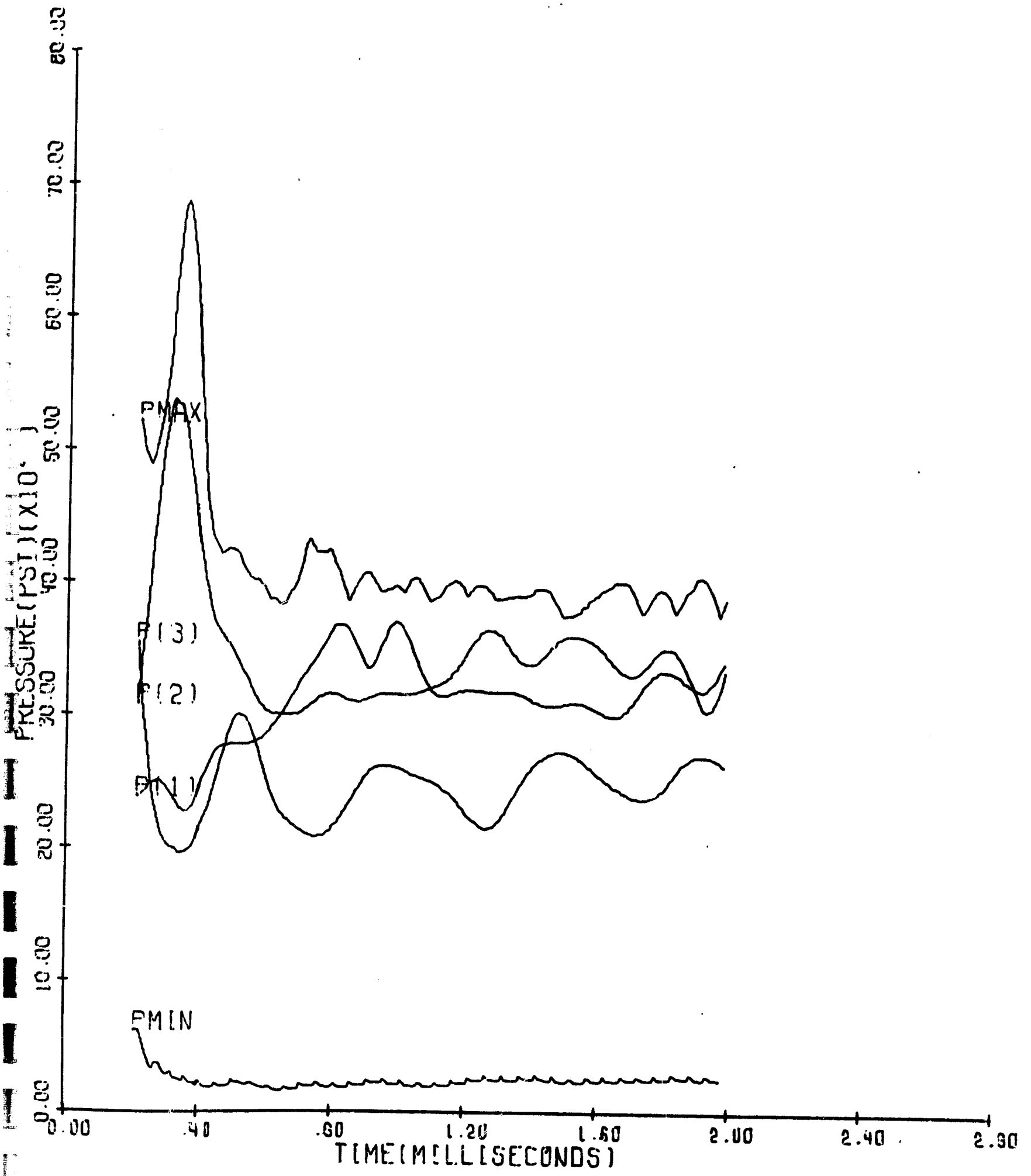

FIG. 16

KUSHIDA POP WITH SHUTTER AP=P**0.45

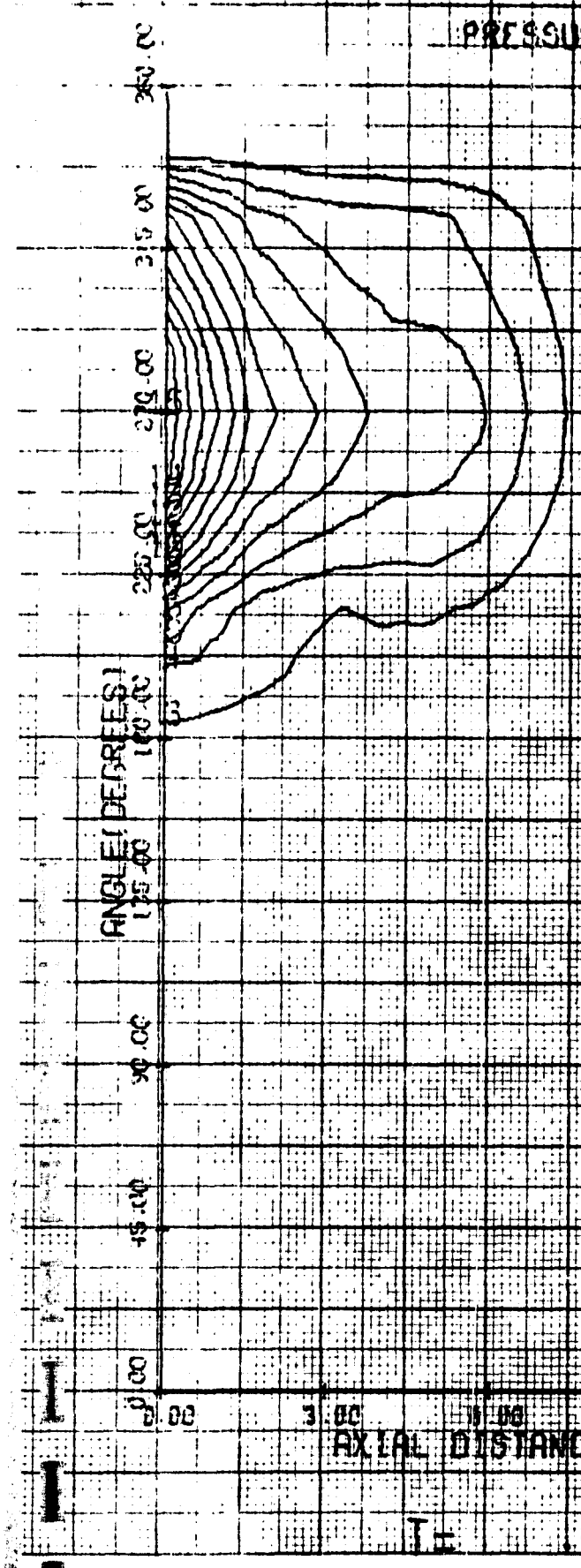

T= .048 MILLISECONDS

ISOBAR	PRESSURE(PSI)
1	24,406
2	209,543
3	394,679
4	579,816
5	764,953
6	950,089
7	1135,226
8	1320,362
9	1505,499
10	1690,636
11	1875,772
12	2060,909
13	2246,046
14	2431,182
15	2616,319

PREF=REFERENCE PRESSURE = 300.00 PSI
AREF=REFERENCE SOUND SPEED= 3221.7 FT/SEC
R =CHAMBER RADIUS = .45830 FEET
TREF=REFERENCE TIME=R/AREF=.0001423 SEC

T/TREF= .33835

ISOBAR	PRESSURE/PREF
1	.081
2	.698
3	1.316
4	1.933
5	2.550
6	3.167
7	3.784
8	4.401
9	5.018
10	5.635
11	6.253
12	6.870
13	7.487
14	8.104
15	8.721

FIG.17

JUDSON BIGELOW, INC.

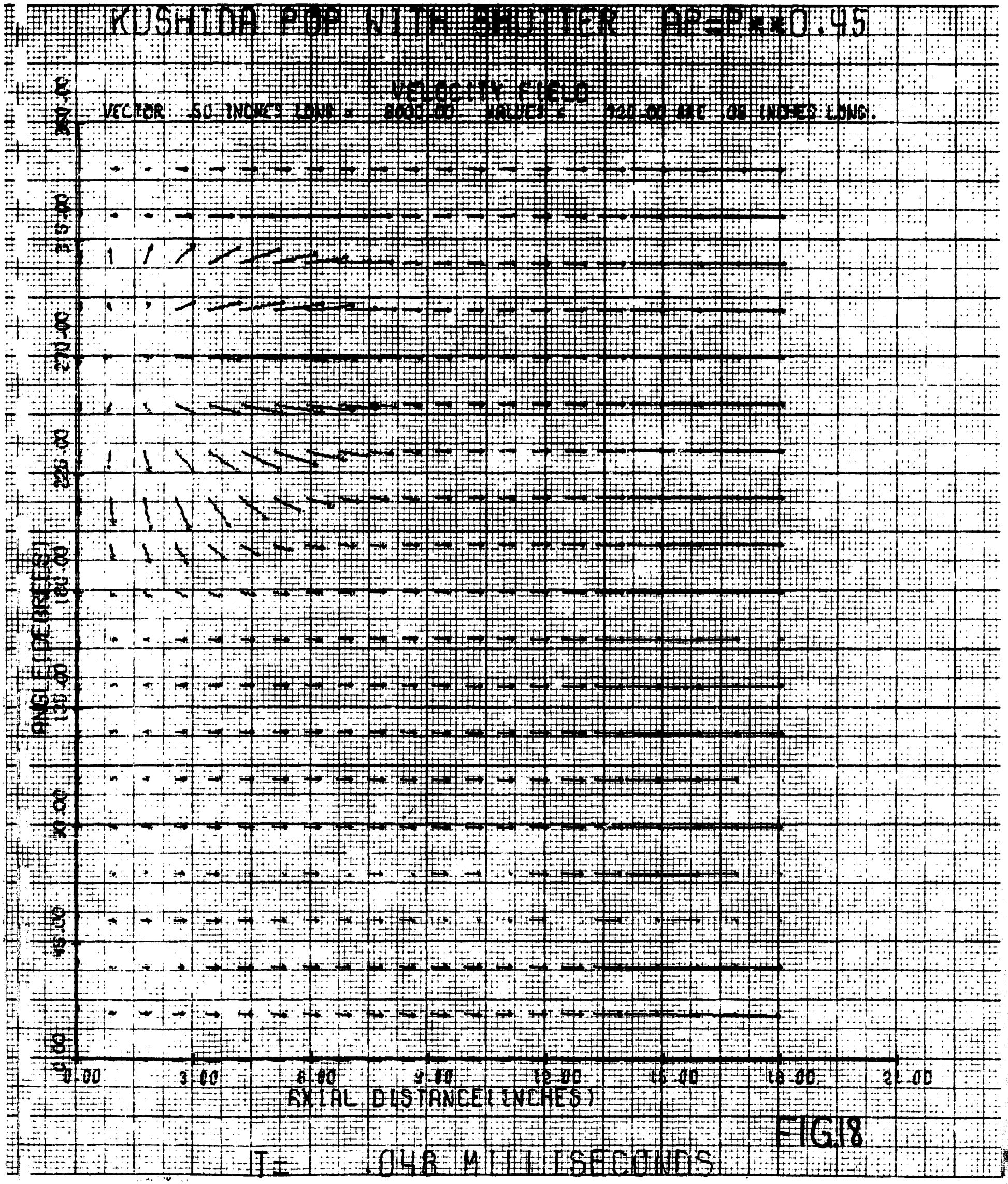
KUSHION FOR WITH SHUTTER AR=P**0.45
VELOCITY FIELD
VECTOR .50 INCHES LONG = 8000.00 VALUES = 120.00 ARE .08 INCHES LONG.
ANGLE FROM CENTERLINE
360.00
315.00
270.00
225.00
180.00
135.00
90.00
45.00
0.00
0.00
3.00
6.00
9.00
12.00
15.00
18.00
21.00
AXIAL DISTANCE(INCHES)
T= .048 MILLISECONDS

FIG.18

KUSRIDA PDP WITH SHUTTER AR_P=0.45

PRESSURE (BOBARS)

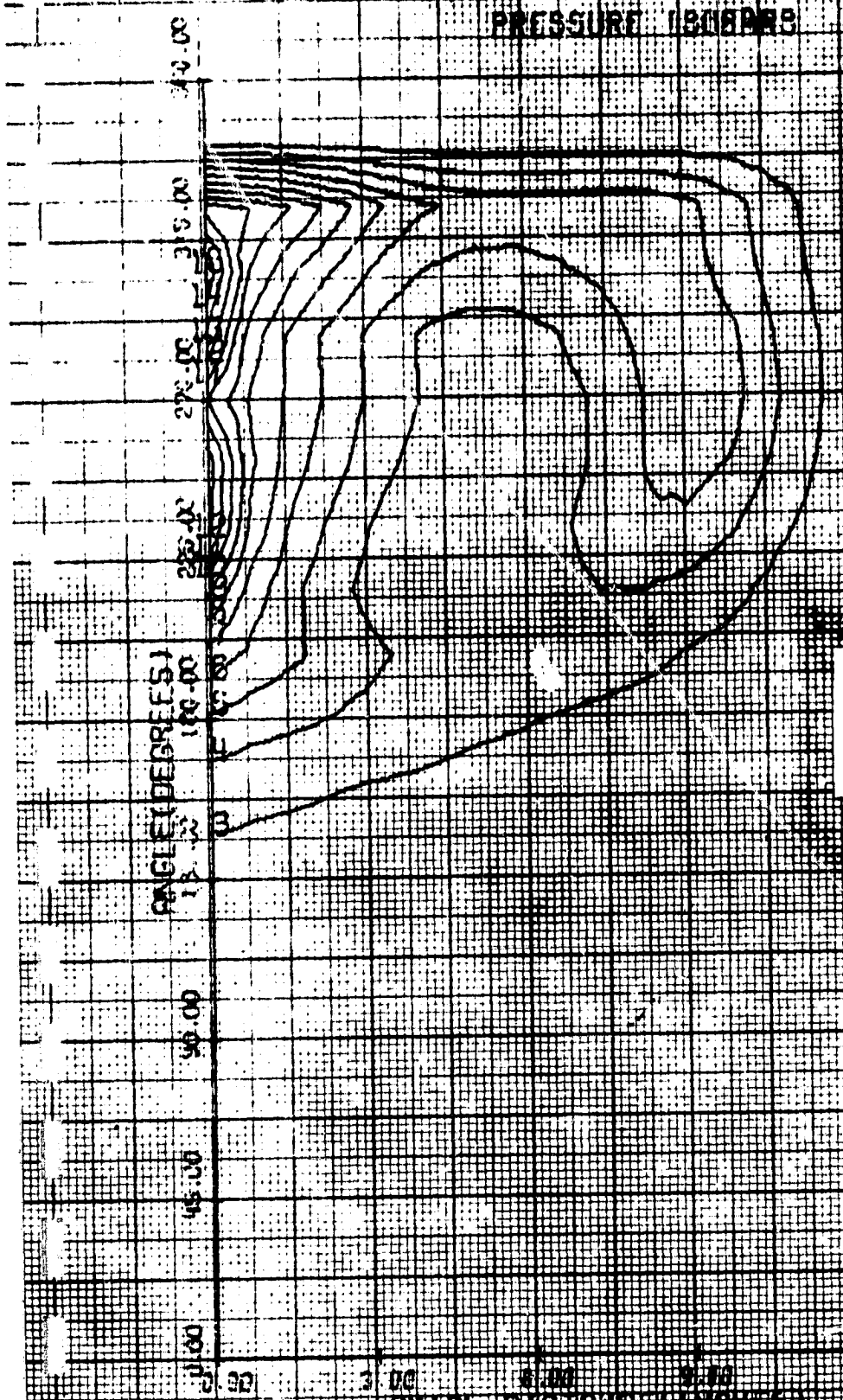

T= .094 MILLISECONDS

ISOBAR	PRESSURE(PSI)
1	25,154
2	170,377
3	315,601
4	460,824
5	606,048
6	751,272
7	896,495
8	1041,719
9	1186,942
10	1332,166
11	1477,389
12	1622,613
13	1767,837
14	1913,060
15	2058,284

PREF=REFERENCE PRESSURE = 300.00 PSI
AREF=REFERENCE SOUND SPEED= 3220.7 FT/SEC
R =CHAMBER RADIUS = .45830 FEET
TREF=REFERENCE TIME=R/AREF=.0001423 SEC

T/TREF= .66008

ISOBAR	PRESSURE/PREF
1	.084
2	.568
3	1.052
4	1.536
5	2.020
6	2.504
7	2.988
8	3.472
9	3.956
10	4.441
11	4.925
12	5.409
13	5.893
14	6.377
15	6.861

FIG 19

(CALCOM-02)

JUDSON BIGELOW, INC.

KUSHIDA POP WITH SHUTTER AP=P**0.45

VELOCITY FIELD

VECTOR .50 INCHES LONG = 0010.00 VALUES 720.00 ARE .06 INCHES LONG.

ANGLE FROM LEADING EDGE

0.00
90.00
180.00
225.00
270.00
315.00
360.00

0.00 3.00 6.00 9.00 12.00 15.00 18.00 21.00

AXIAL DISTANCE (INCHES)

T= .094 MILLISECONDS

FIG. 20

KUSHIDA POP WITH SHUTTER AP=P**0.45

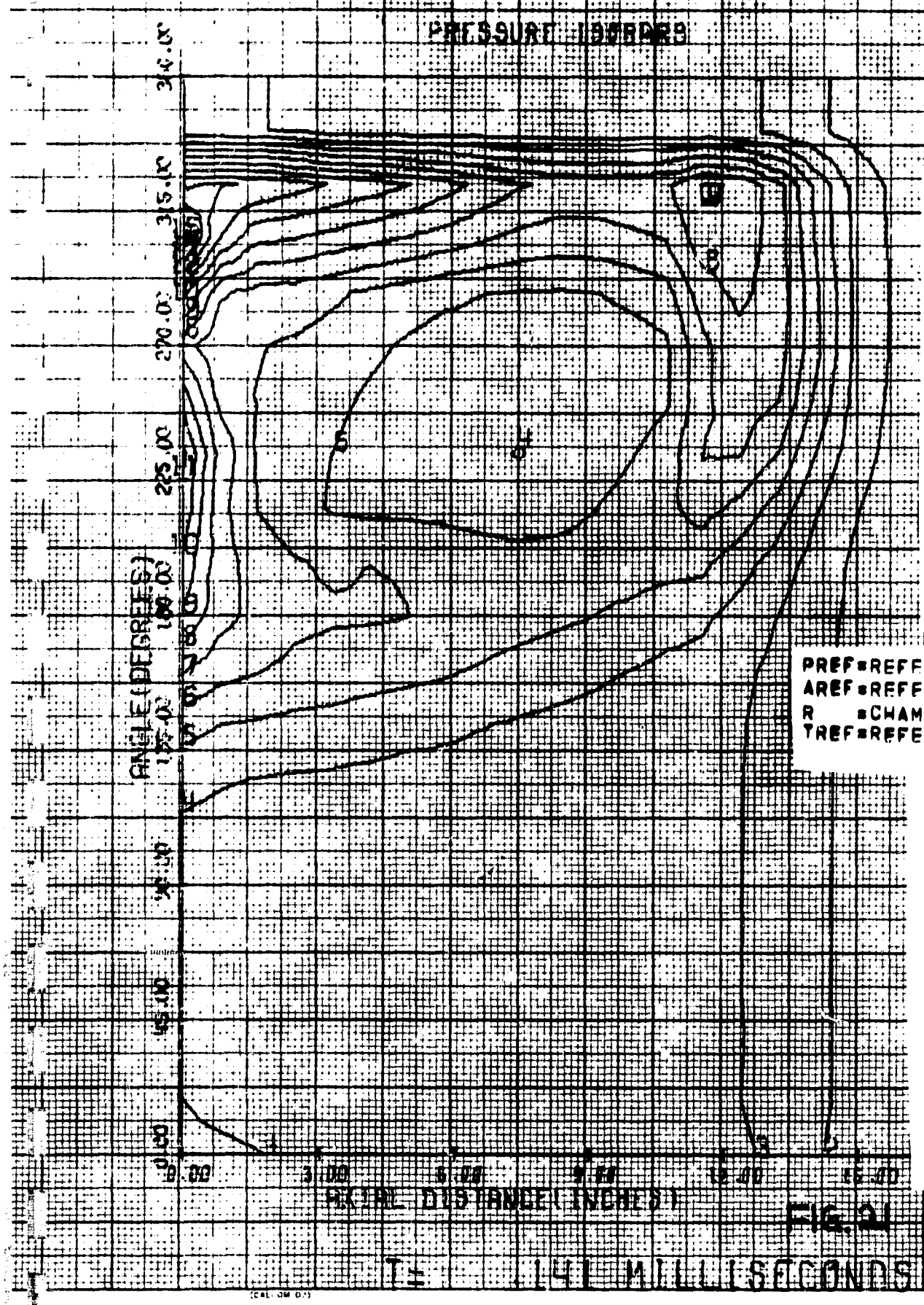

T= .141 MILLISECONDS

ISOBAR	PRESSURE(PSI)
1	-3,218
2	91,172
3	185,562
4	279,952
5	374,343
6	468,733
7	563,123
8	657,513
9	751,904
10	846,294
11	940,684
12	1035,074
13	1129,465
14	1223,855
15	1318,245

PREF=REFERENCE PRESSURE = 300,00 PSI
AREF=REFERENCE SOUND SPEED= 3220,7 FT/SEC
R =CHAMBER RADIUS = ,45830 FEET
TREF=REFERENCE TIME=R/AREF=,0001423 SEC

T/TREF= ,99096

ISOBAR	PRESSURE/PREF
1	-,011
2	,304
3	,619
4	,933
5	1,248
6	1,562
7	1,877
8	2,192
9	2,506
10	2,821
11	3,136
12	3,450
13	3,765
14	4,080
15	4,394

FIG. 21

T= .141 MILLISECONDS

JUDSON BIGELOW, INC.

KUSHLOA PORT WITH SHUTTER A'=P**0.5

VELOCITY FIELD

VECTOR 5.: INCHES LONG = 6000.00. VALUES > 120.00 ARE OF INCHES LONG.

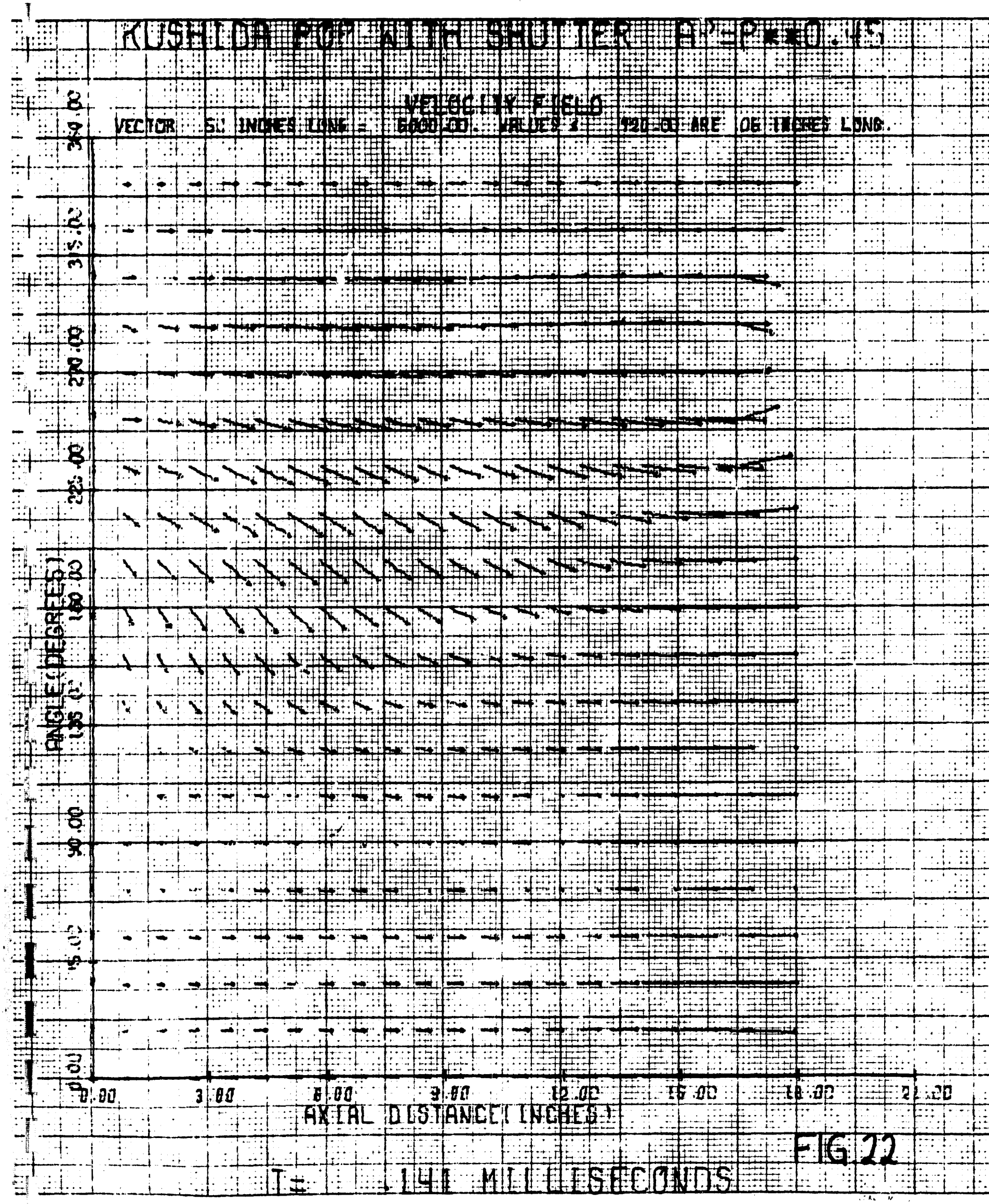

FIG.22

T= 141 MILLISECONDS

KUSHIDA PØP WITH SHUTTER A=P=0.45

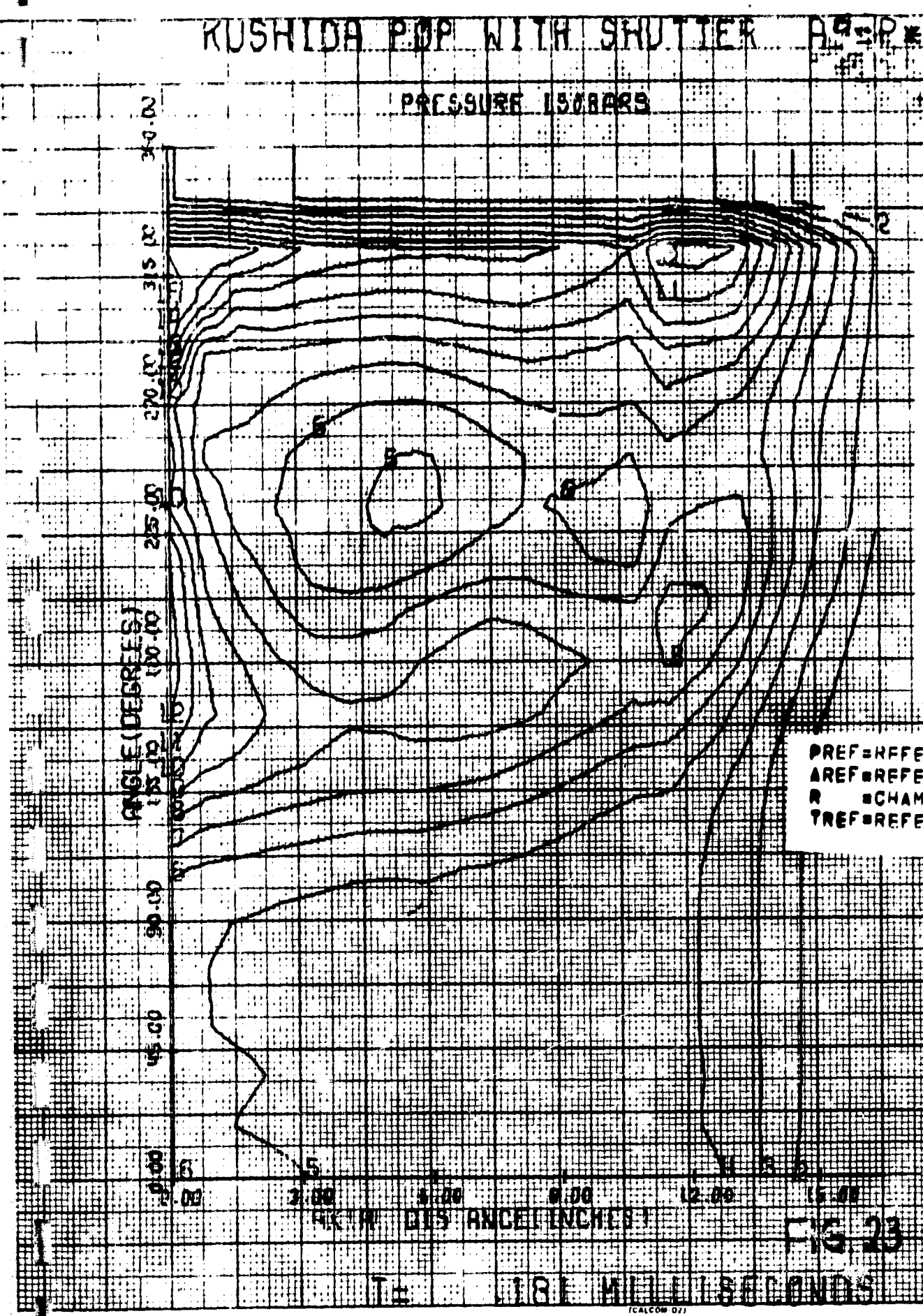

T= .181 MILLISECONDS

ISOBAR	PRESSURE(PSI)
1	25,154
2	80,908
3	136,662
4	192,416
5	248,170
6	303,925
7	359,679
8	415,433
9	471,187
10	526,941
11	582,696
12	638,450
13	694,204
14	749,958
15	805,712

PREF=REFERENCE PRESSURE = 300.00 PSI
AREF=REFERENCE SOUND SPEED= 3220.7 FT/SEC
R =CHAMBER RADIUS = .45830 FEET
TREF=REFERENCE TIME=R/AREF=.0001423 SEC

T/TREF= 1.26973

ISOBAR	PRESSURE/PREF
1	.084
2	.270
3	.456
4	.641
5	.827
6	1.013
7	1.199
8	1.385
9	1.571
10	1.756
11	1.942
12	2.128
13	2.314
14	2.500
15	2.686

FIG 23

KUSHIDA PUP WITH SHUTTER AR=P*R0.45

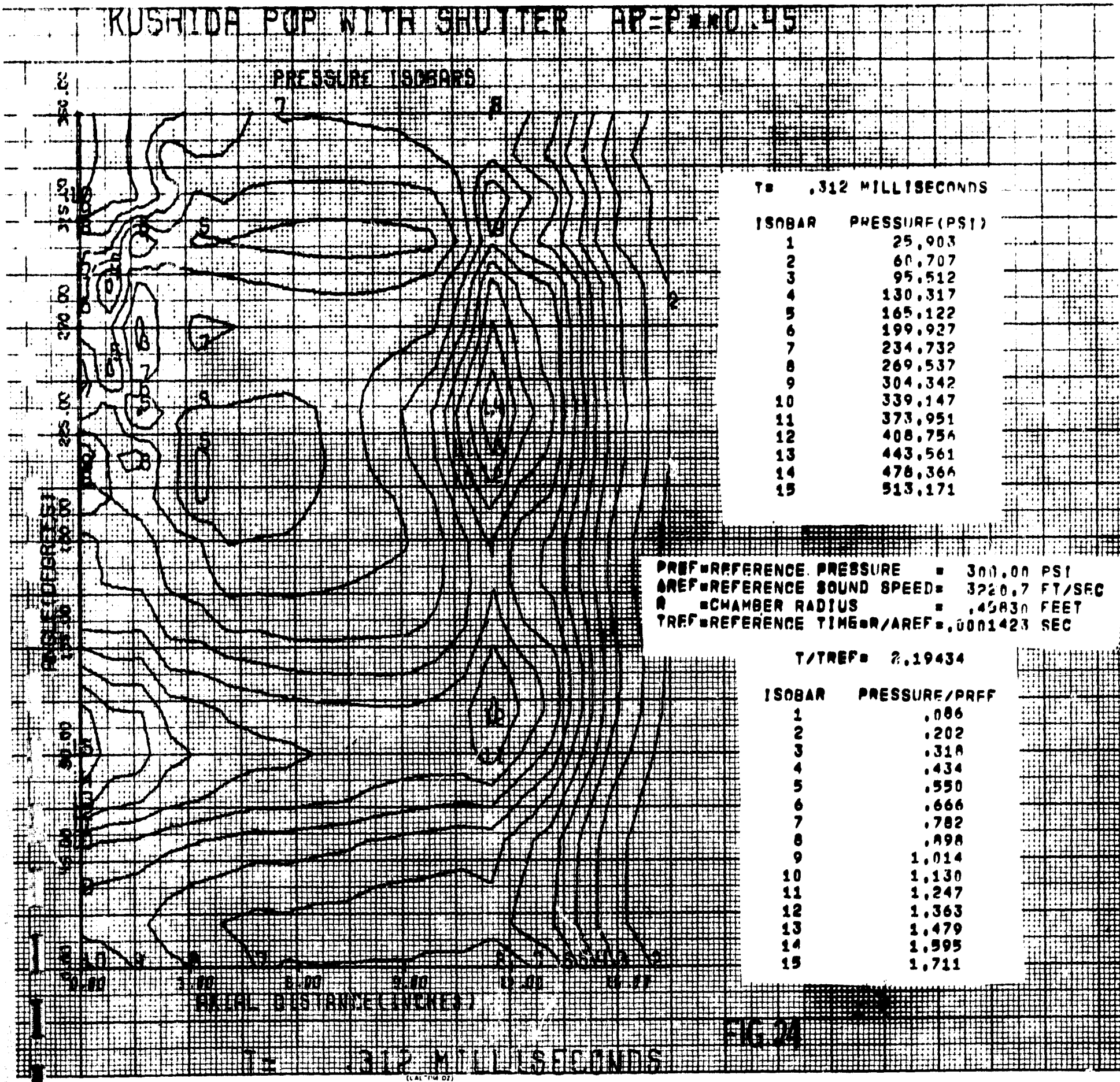

T= .312 MILLISECONDS

ISOBAR	PRESSURE(PSI)
1	25.903
2	60.707
3	95.512
4	130.317
5	165.122
6	199.927
7	234.732
8	269.537
9	304.342
10	339.147
11	373.951
12	408.756
13	443.561
14	478.366
15	513.171

PREF=REFERENCE PRESSURE = 300.00 PSI
AREF=REFERENCE SOUND SPEED= 3220.7 FT/SEC
R =CHAMBER RADIUS = .45830 FEET
TREF=REFERENCE TIME=R/AREF=.0001423 SEC

T/TREF= 2.19434

ISOBAR	PRESSURE/PREF
1	.086
2	.202
3	.318
4	.434
5	.550
6	.666
7	.782
8	.898
9	1.014
10	1.130
11	1.247
12	1.363
13	1.479
14	1.595
15	1.711

FIG 24

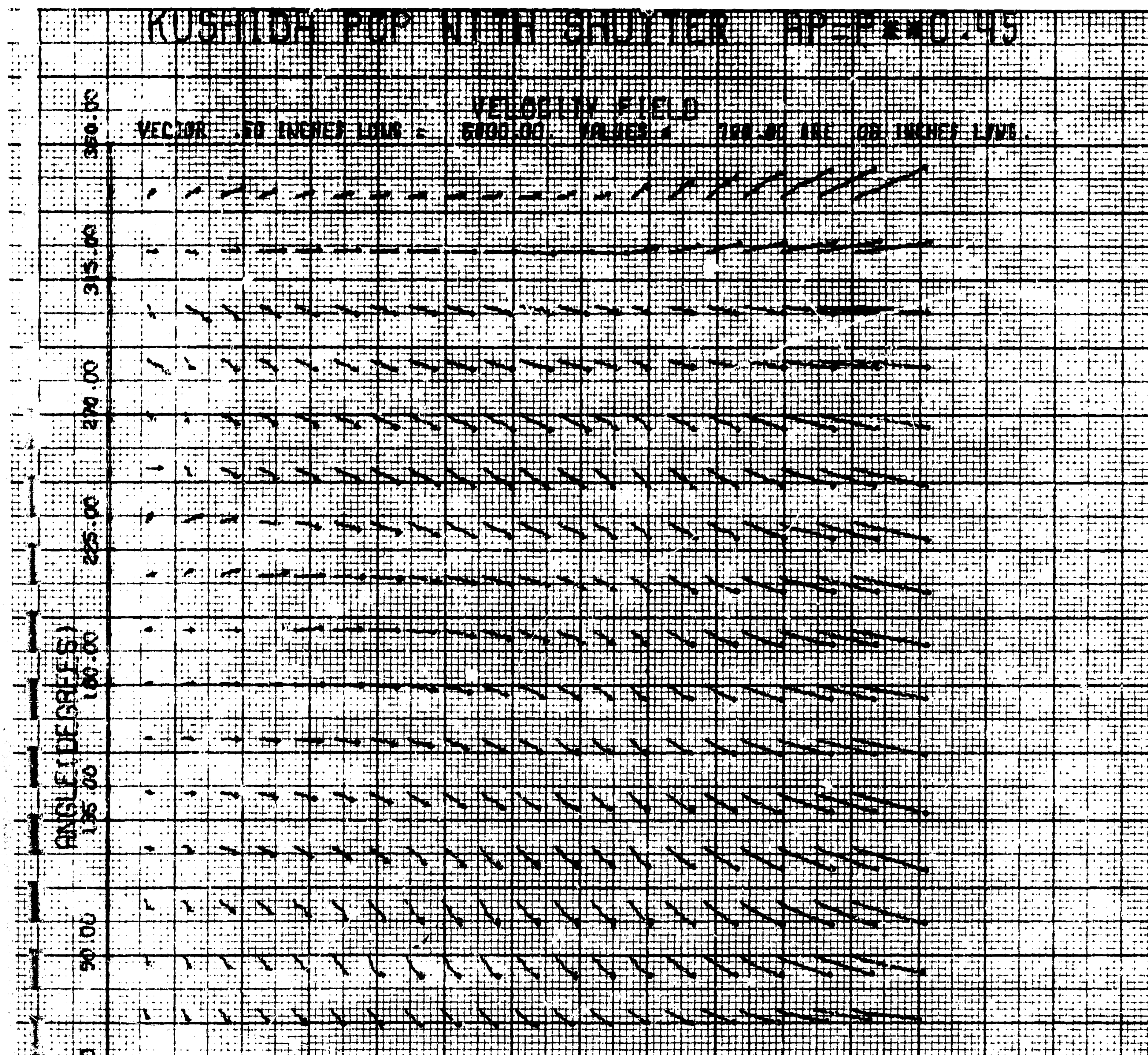

FIG. 25

T= 312 MILLISECONDS

KUSHIDA POP WITH SHUTTER AP=P**0.45

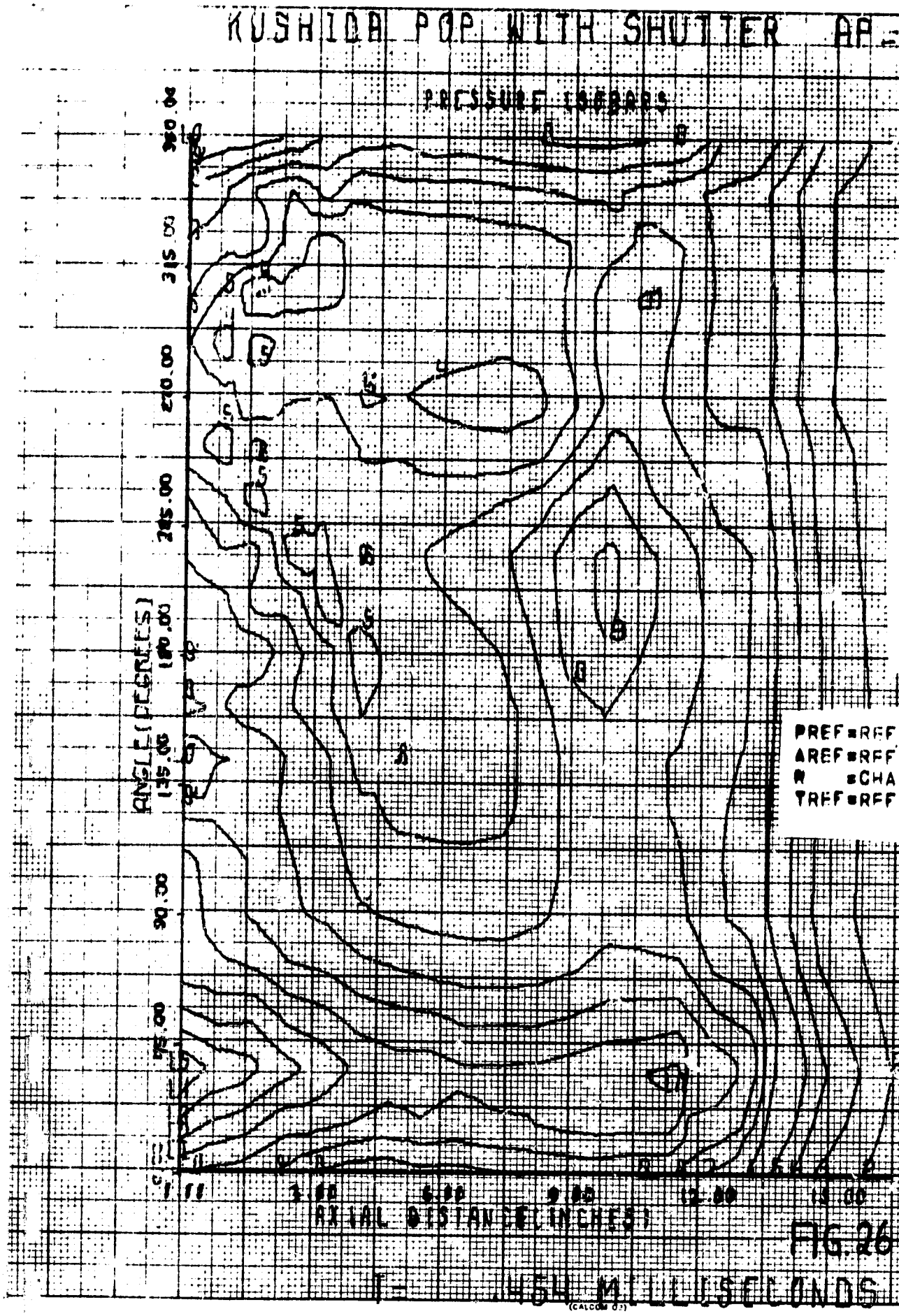

T= .454 MILLISECONDS

ISOBAR	PRESSURE(PSI)
1	17,946
2	56,454
3	94,963
4	133,471
5	171,979
6	210,487
7	248,995
8	287,503
9	326,011
10	364,519
11	403,027
12	441,535
13	480,044
14	518,552
15	557,060

PREF=REFERENCE PRESSURE = 300,00 PSI
AREF=REFERENCE SOUND SPEED= 3220,7 FT/SEC
R =CHAMBER RADIUS = ,45830 FEET
TREF=REFERENCE TIME=R/AREF=,0001423 SEC

T/TREF= 3,19212

ISOBAR	PRESSURE/PREF
1	,060
2	,188
3	,317
4	,445
5	,573
6	,702
7	,830
8	,958
9	1,087
10	1,215
11	1,343
12	1,472
13	1,600
14	1,729
15	1,857

FIG. 26

T= .454 MILLISECONDS

(CALCOMP 07)

KUSHIDA POP WITH SHUTTER AP=P*=0.45

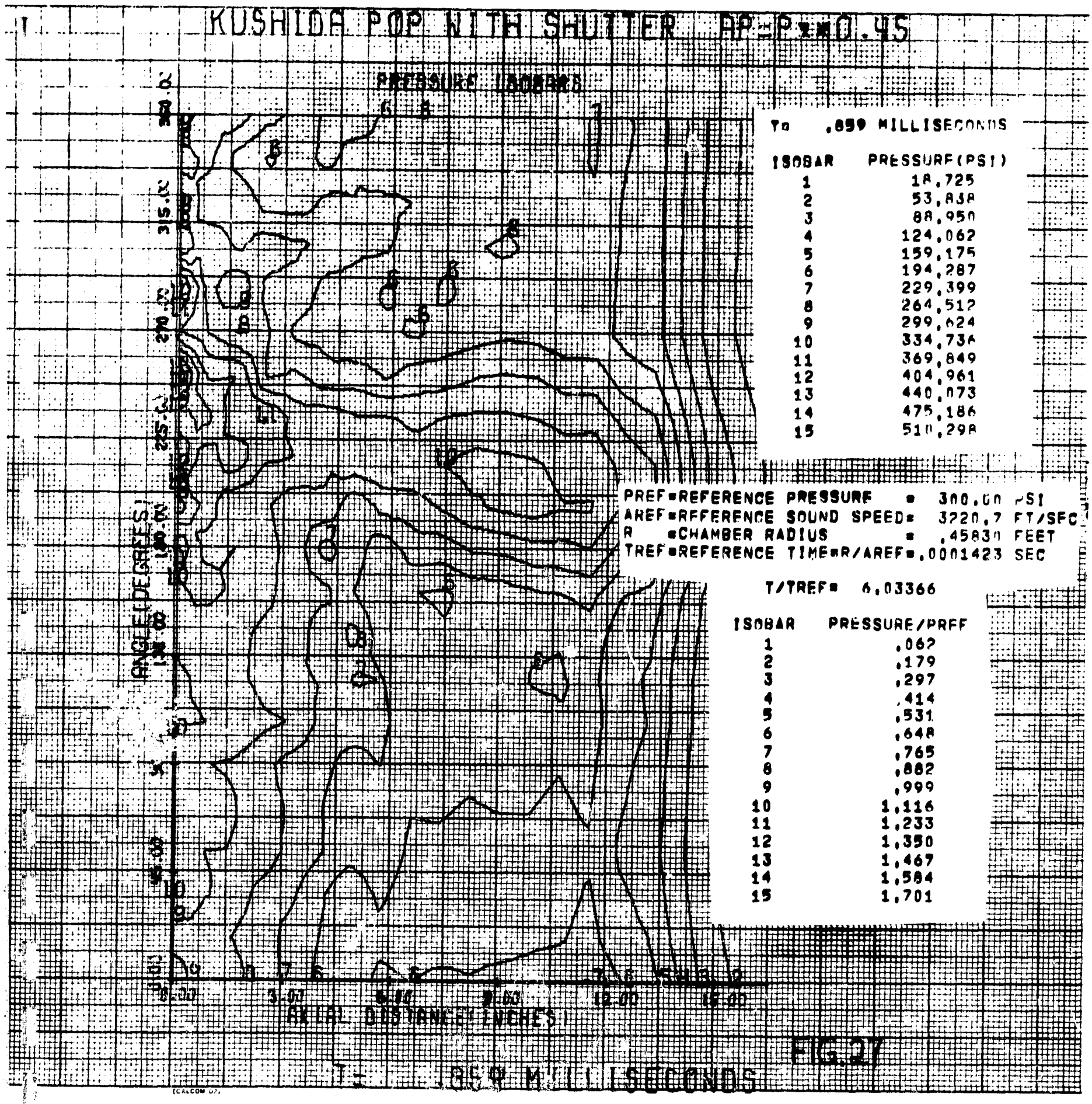

To ,859 MILLISECONDS

ISOBAR	PRESSURE(PSI)
1	18,725
2	53,838
3	88,950
4	124,062
5	159,175
6	194,287
7	229,399
8	264,512
9	299,624
10	334,736
11	369,849
12	404,961
13	440,073
14	475,186
15	510,298

PREF=REFERENCE PRESSURE = 300.00 PSI
AREF=REFERENCE SOUND SPEED= 3220.7 FT/SEC
R =CHAMBER RADIUS = .45830 FEET
TREF=REFERENCE TIME=R/AREF=.0001423 SEC

T/TREF= 6.03366

ISOBAR	PRESSURE/PREF
1	.062
2	.179
3	.297
4	.414
5	.531
6	.648
7	.765
8	.882
9	.999
10	1.116
11	1.233
12	1.350
13	1.467
14	1.584
15	1.701

T= .859 MILLISECONDS

FIG.27

JUDSON BIGELOW, INC.

56373

KUSHIDA POP WITH SHUTTER AP-P*D.45

VECTOR FIELD

VECTOR 50 INCHES LONG = 8000.00 VALUES = 720.00 ARE 60 INCHES LONG

ANGLE IN DEGREES

270.00
225.00
180.00
135.00
90.00
45.00
0.00

0.00 3.00 6.00 9.00 12.00 15.00 18.00 21.00

AXIAL DISTANCE (INCHES)

FIG. 28

T= .858 MILLISECONDS

HUDSON PIGFLOW, INC.

KUSHIDA POP WITH SHUTTER AP=P**0.45

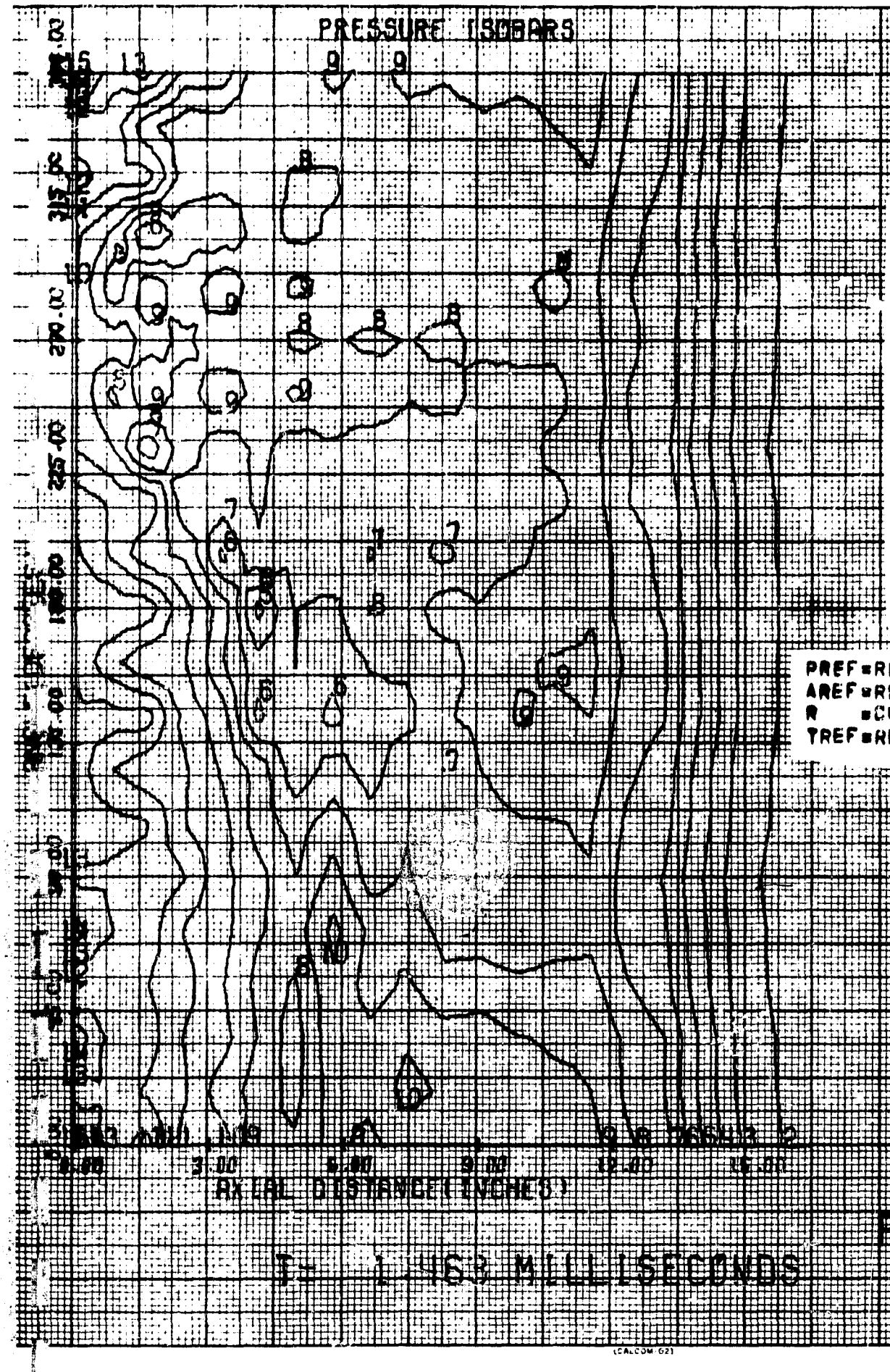

T= 1.463 MILLISECONDS

ISOBAR	PRESSURE(PSI)
1	22,764
2	51,760
3	80,753
4	109,747
5	138,741
6	167,734
7	196,728
8	225,722
9	254,715
10	283,709
11	312,703
12	341,697
13	370,690
14	399,684
15	428,678

PREF=REFERENCE PRESSURE = 300.00 PSI
AREF=REFERENCE SOUND SPEED= 3220.7 FT/SEC
R =CHAMBER RADIUS = .45830 FEET
TREF=REFERENCE TIME=R/AREF=.0001423 SEC

T/TREF= 10.28020

ISOBAR	PRESSURE/PREF
1	.076
2	.173
3	.269
4	.366
5	.462
6	.559
7	.656
8	.752
9	.849
10	.946
11	1.042
12	1.139
13	1.236
14	1.332
15	1.429

FIG. 29

(CALCOM-621)

JUDSON BIGELOW, INC.

KUSHIDA POP WITH SHUTTER AP=P**0.45

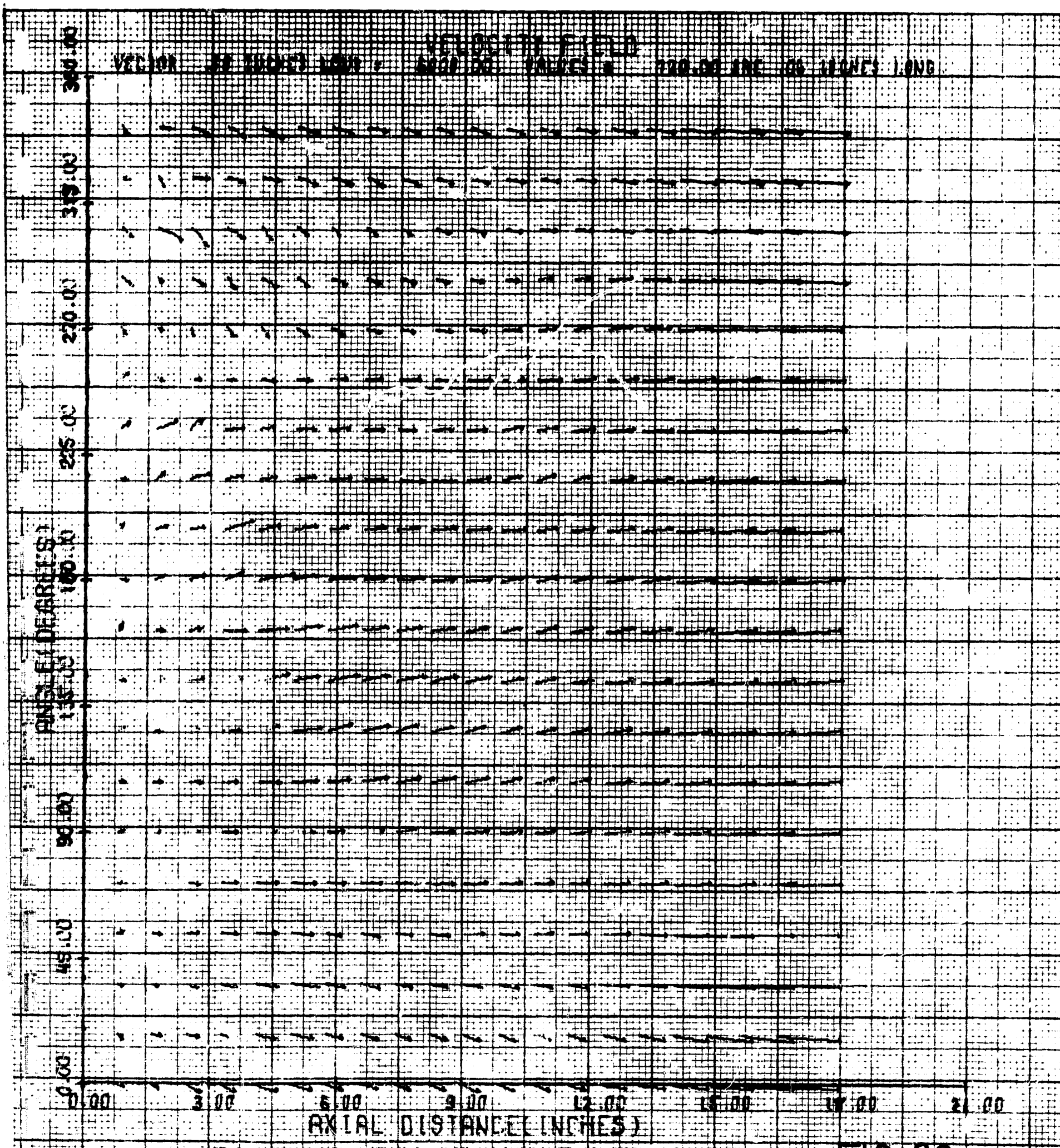

FIG. 30

T = 1.463 MILLISECONDS

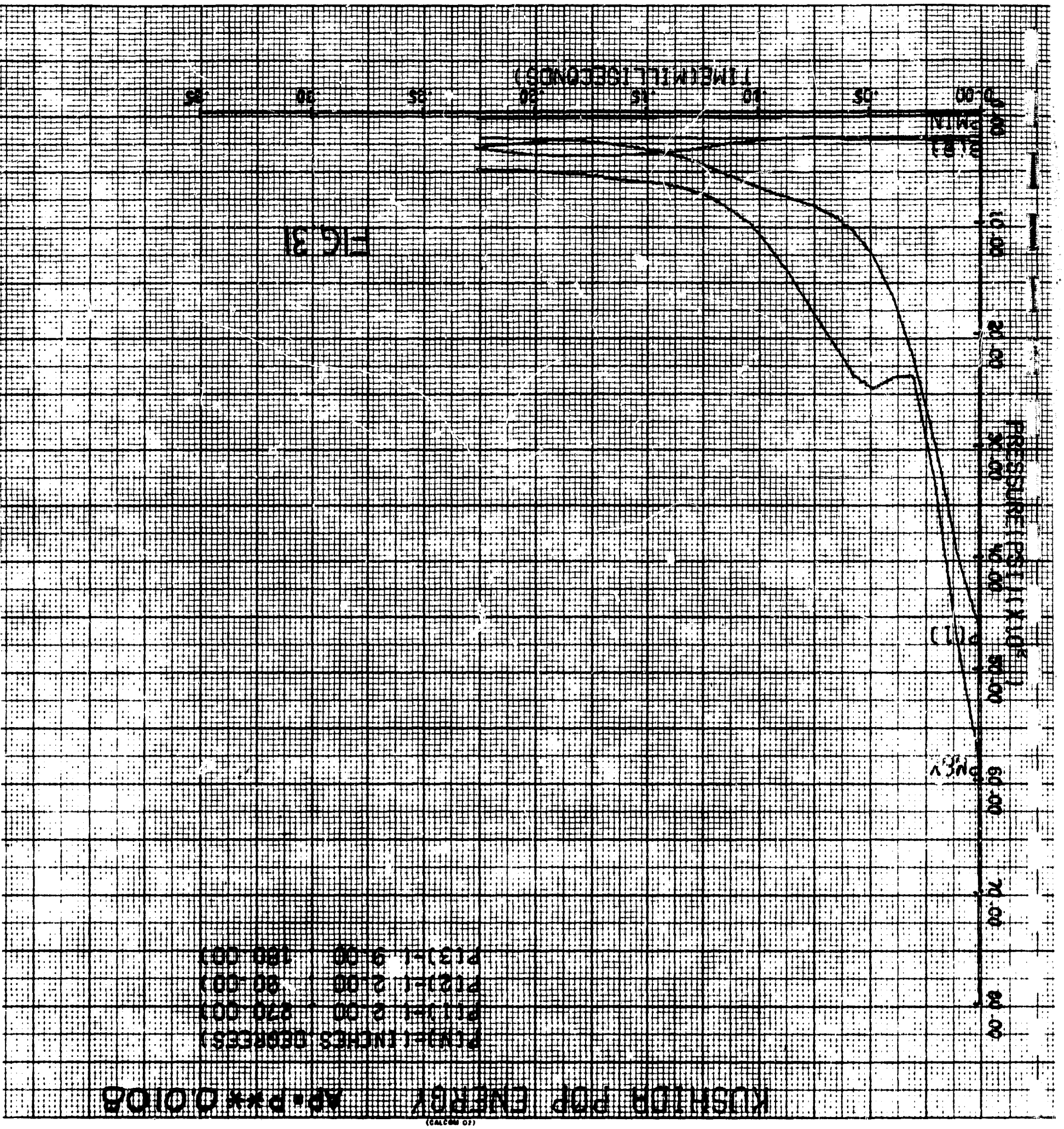
TIME (MILLISECONDS)
PRESSURE (PSIA)
FIG 31
KUSHTOP PDP ENERGY
(CALCOMP 02)

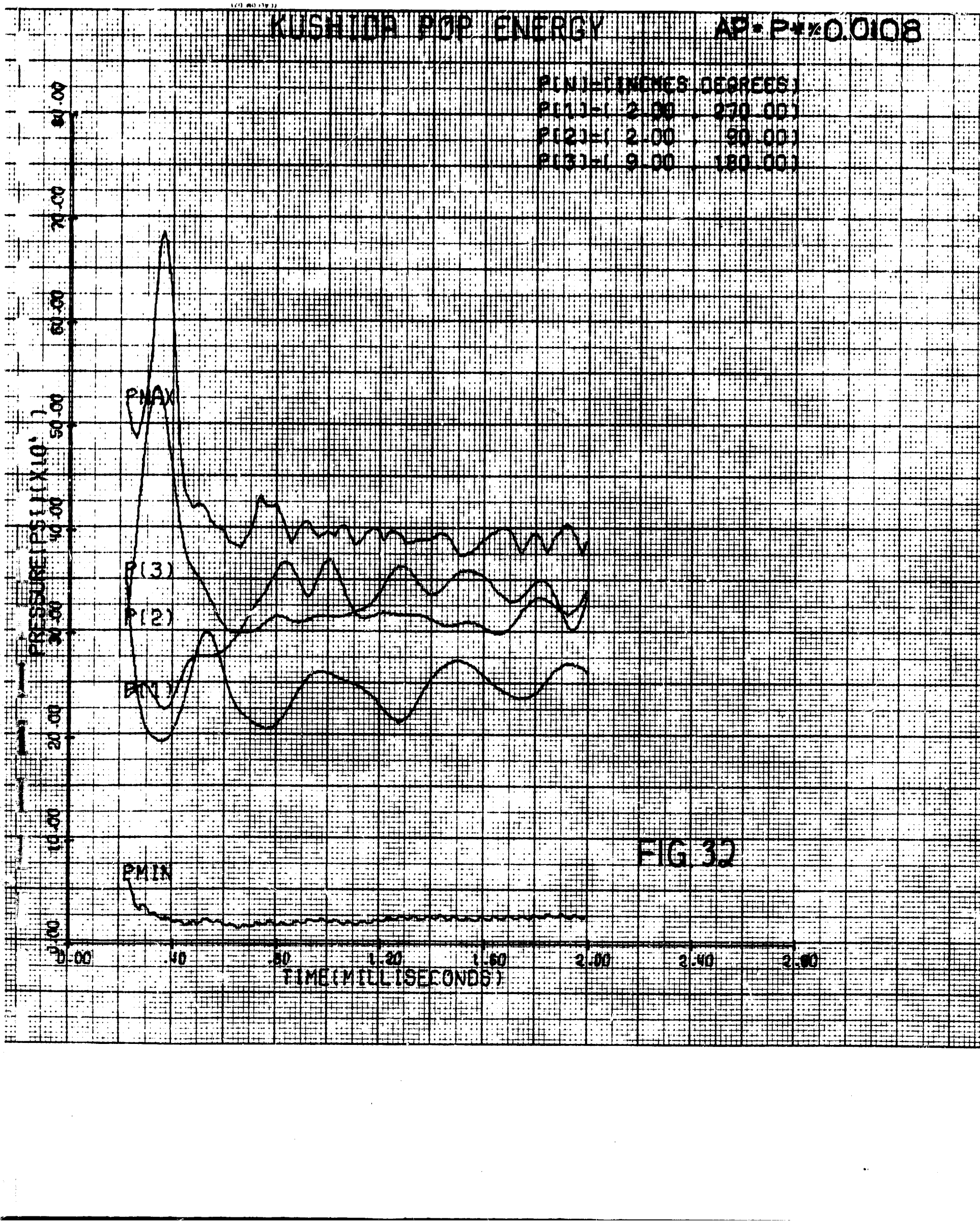
KUSHIDA POP ENERGY
AP • P+=0.0108
P[N]=[INCHES DEGREES]
P[1]=[2.00 270.00]
P[2]=[2.00 90.00]
P[3]=[9.00 180.00]
PMAX
P(3)
P(2)
P(1)
PMIN
PRESSURE(PSIA)
TIME(MILLISECONDS)
0.00
.40
.80
1.20
1.60
2.00
2.40
2.80
10.00
20.00
30.00
40.00
50.00
60.00
70.00
80.00

FIG 32

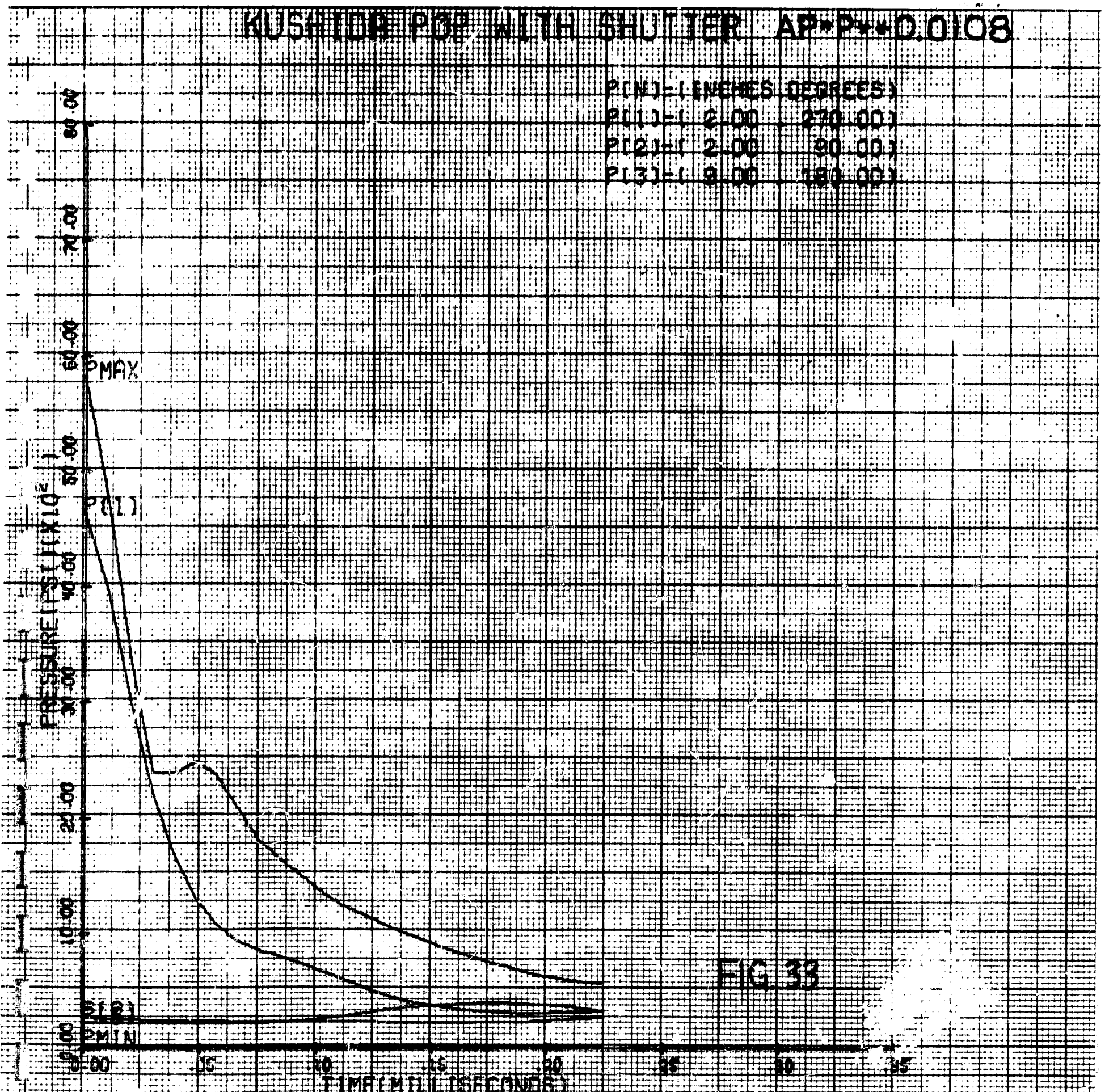
KUSHIOR POP WITH SHUTTER AP=P+=0.0108
P(N)=(INCHES,DEGREES)
P(0)=(0.00, 270.00)
P(2)=(2.00, 90.00)
P(3)=(9.00, 180.00)
PMAX
P(1)
P(2)
PMIN
PRESSURE X10**2 (LB/IN**2)
80.00
70.00
60.00
50.00
40.00
30.00
20.00
10.00
0.00
-10.00
0.00
.05
.10
.15
.20
.25
.30
.35
TIME(MILLISECONDS)

FIG. 33

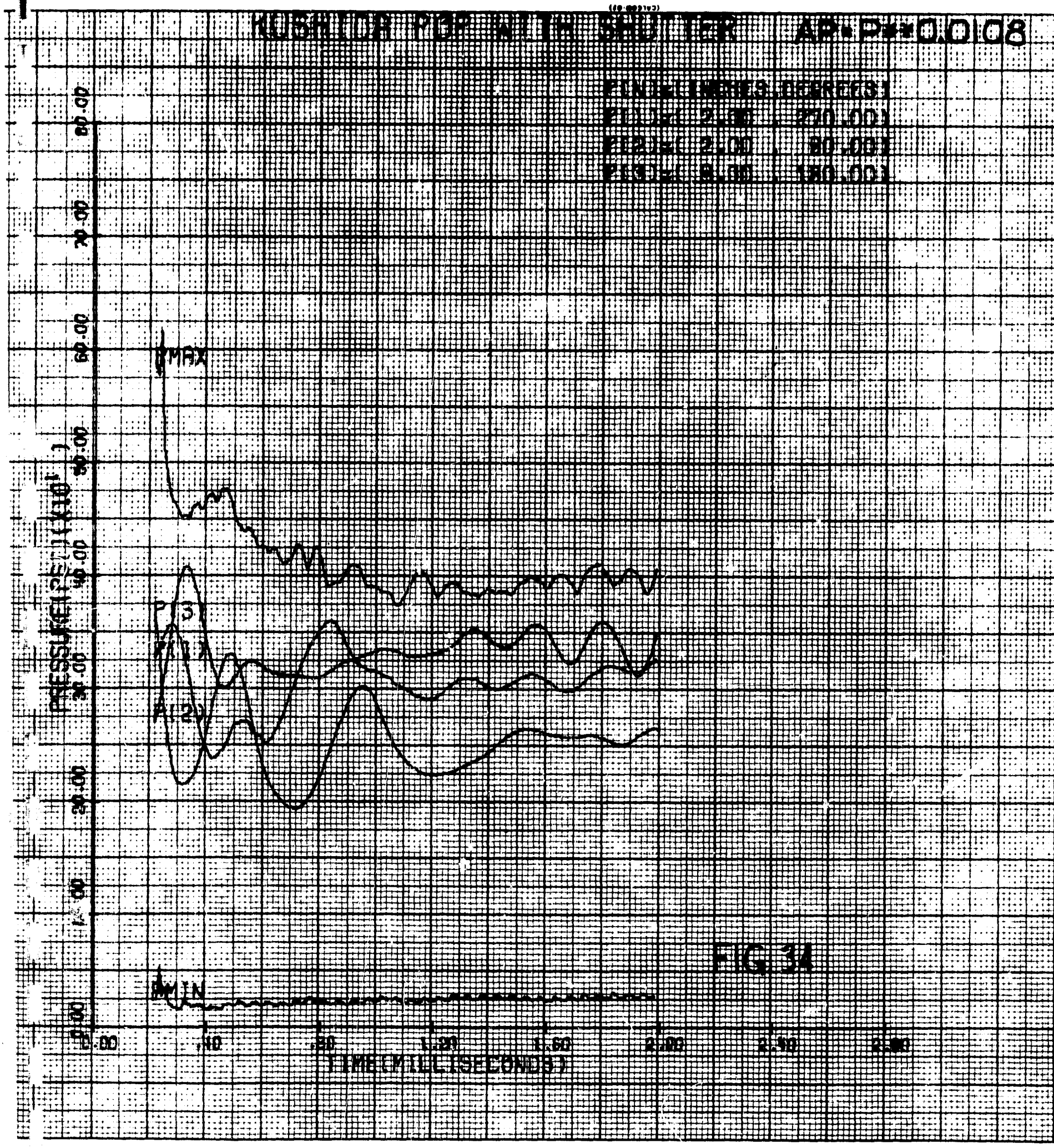
KUSHIOR PGP WITH SHUTTER
AP=P=0.0108
FUNK(METRIC DEGREES)
F(1)=(2.00 , 270.00)
F(2)=(2.00 , 90.00)
F(3)=(8.00 , 180.00)
PMAX
P(3)
P(1)
P(2)
PMIN
PRESSURE(KILOPASCALS)
80.00
70.00
60.00
50.00
40.00
30.00
20.00
10.00
0.00
.40
.80
1.20
1.60
2.00
2.40
2.80
TIME(MILLISECONDS)

FIG 34

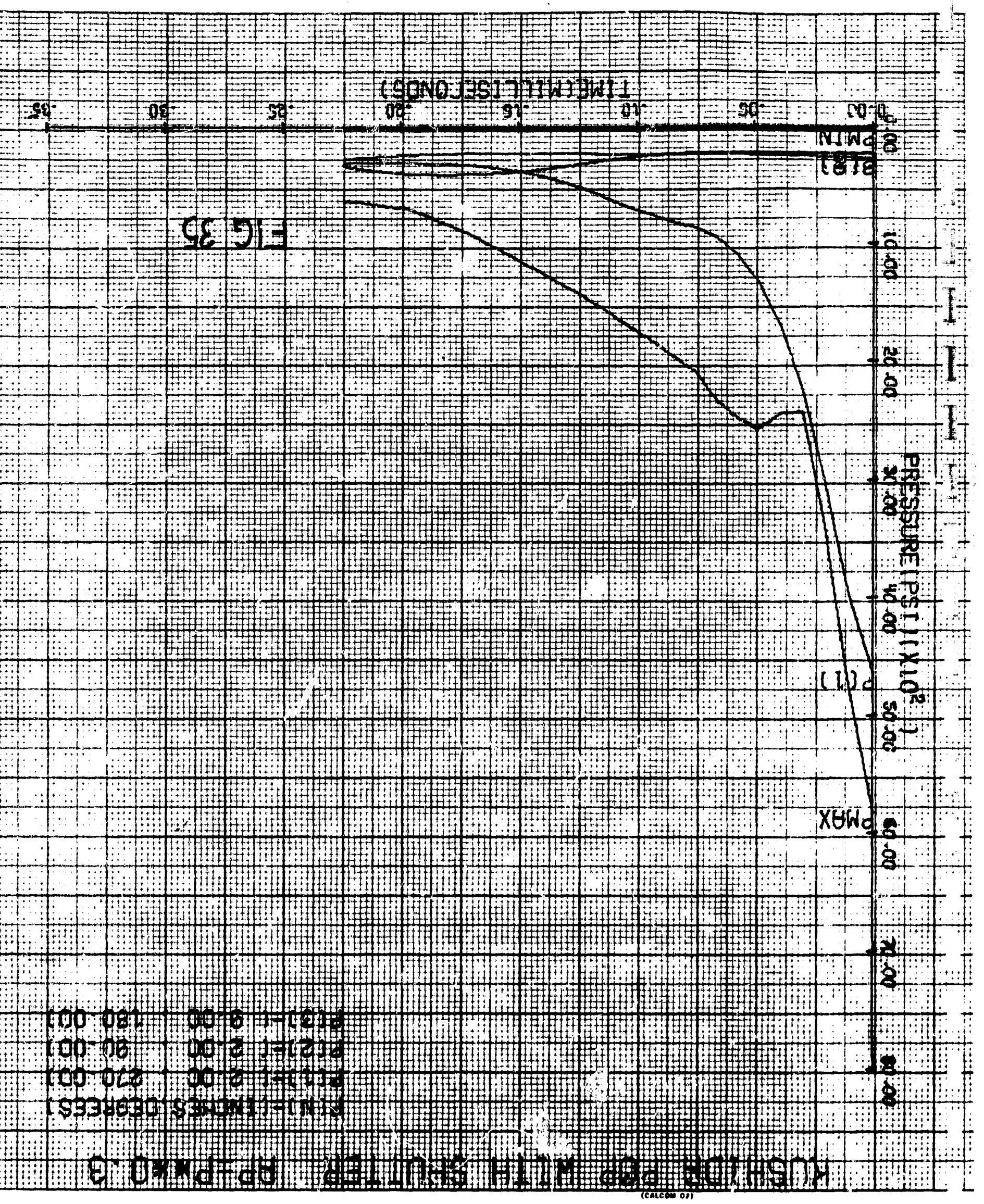

JUDSON BIGELOW, INC.

FIG 36

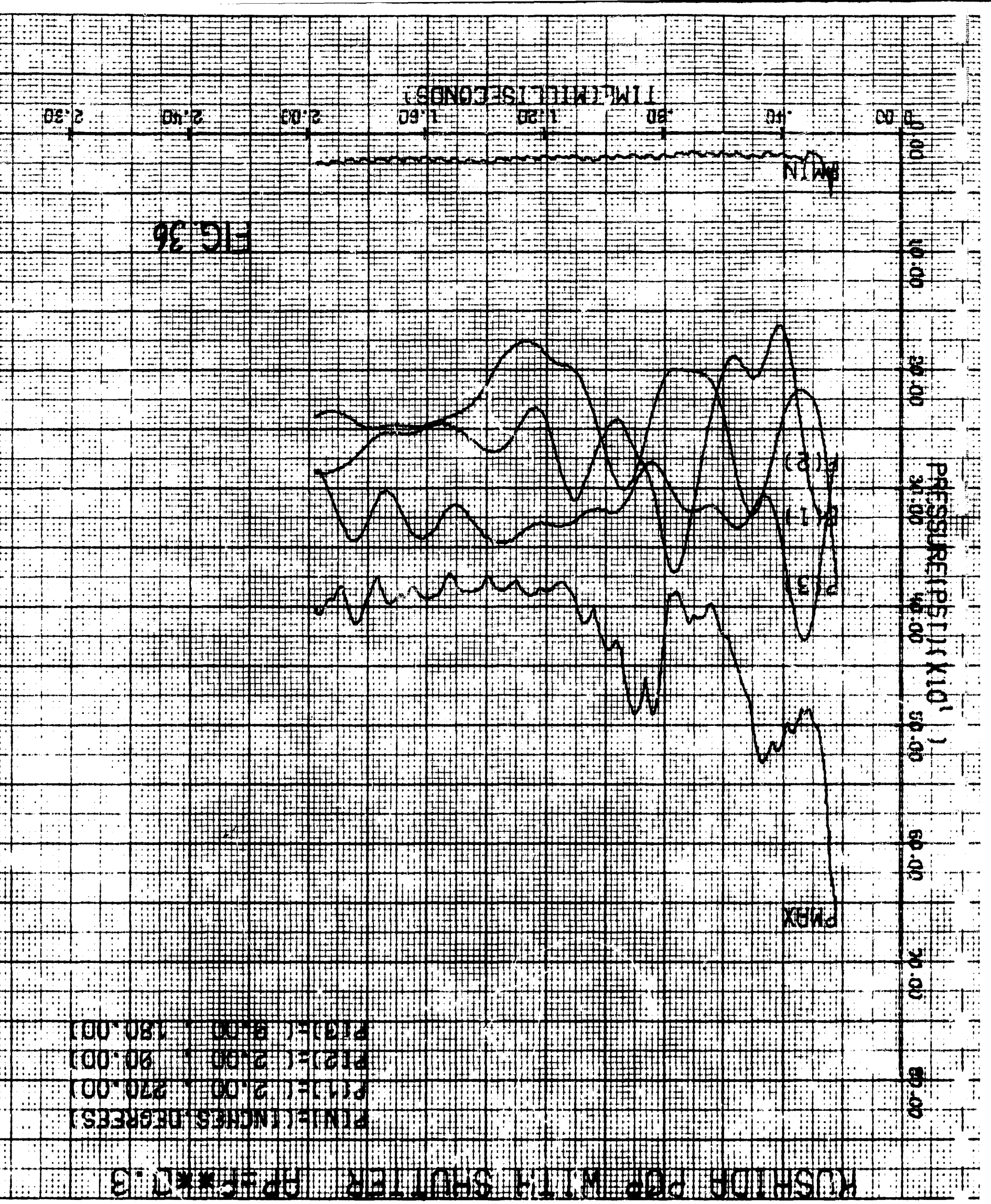

HUDSON BIGELOW, INC.

KUSHIDA POP WITH SHUTTER AP=P**0.45

P(N)=(INCHES.DEGREES)
P(1)=(2.00 . 270.00)
P(2)=(2.00 . 90.00)
P(3)=(9.00 . 180.00)

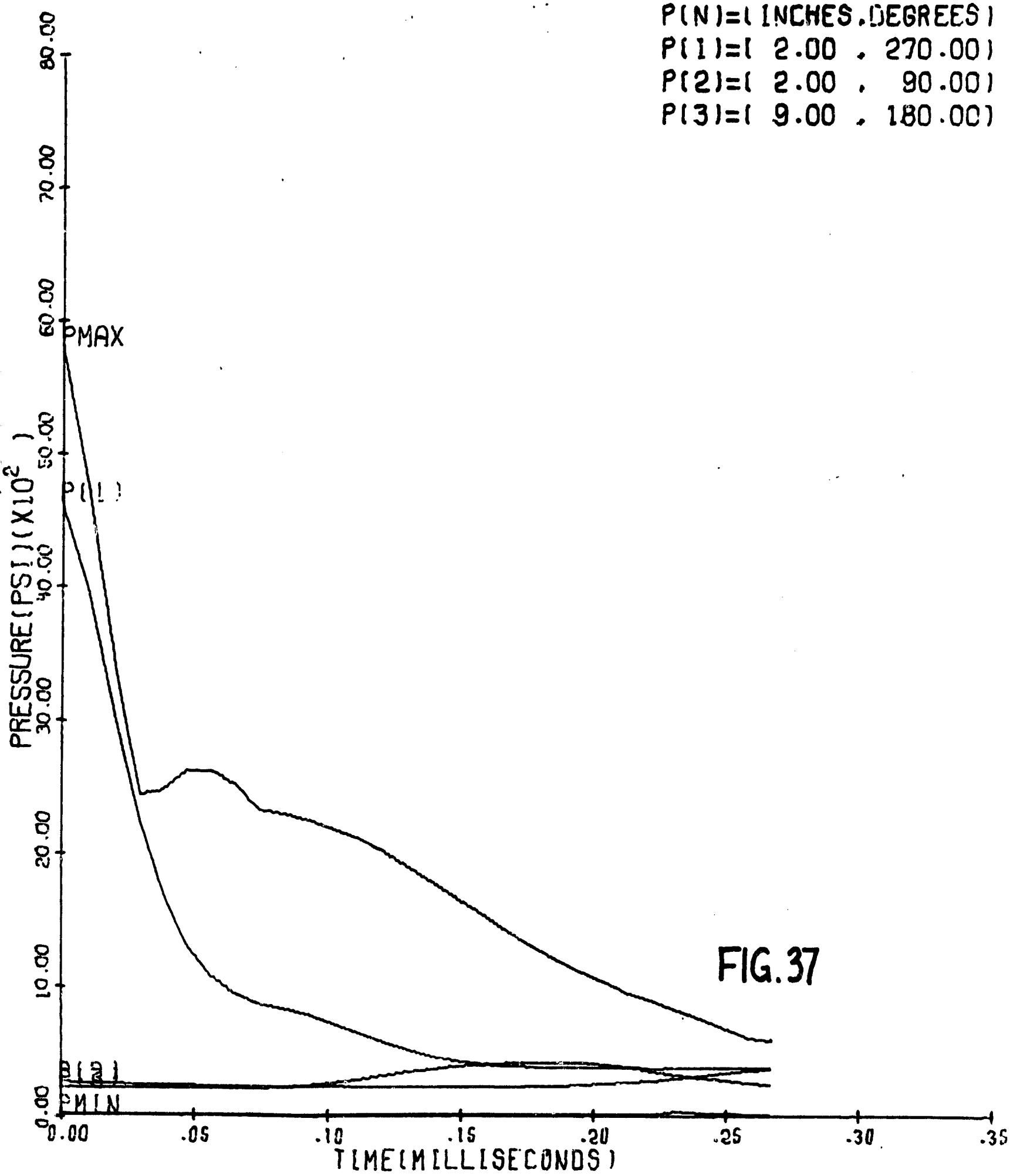

FIG.37

JUDSON BIGELOW, INC.

PMAT

(CALCOM 02)

KUSHIDA POP WITH SHUTTER -SP=P*0.45

P(N)=(INCHES,DEGREES)
P(1)=(2.00 , 270.00)
P(2)=(2.00 , 90.00)
P(3)=(9.00 , 180.00)

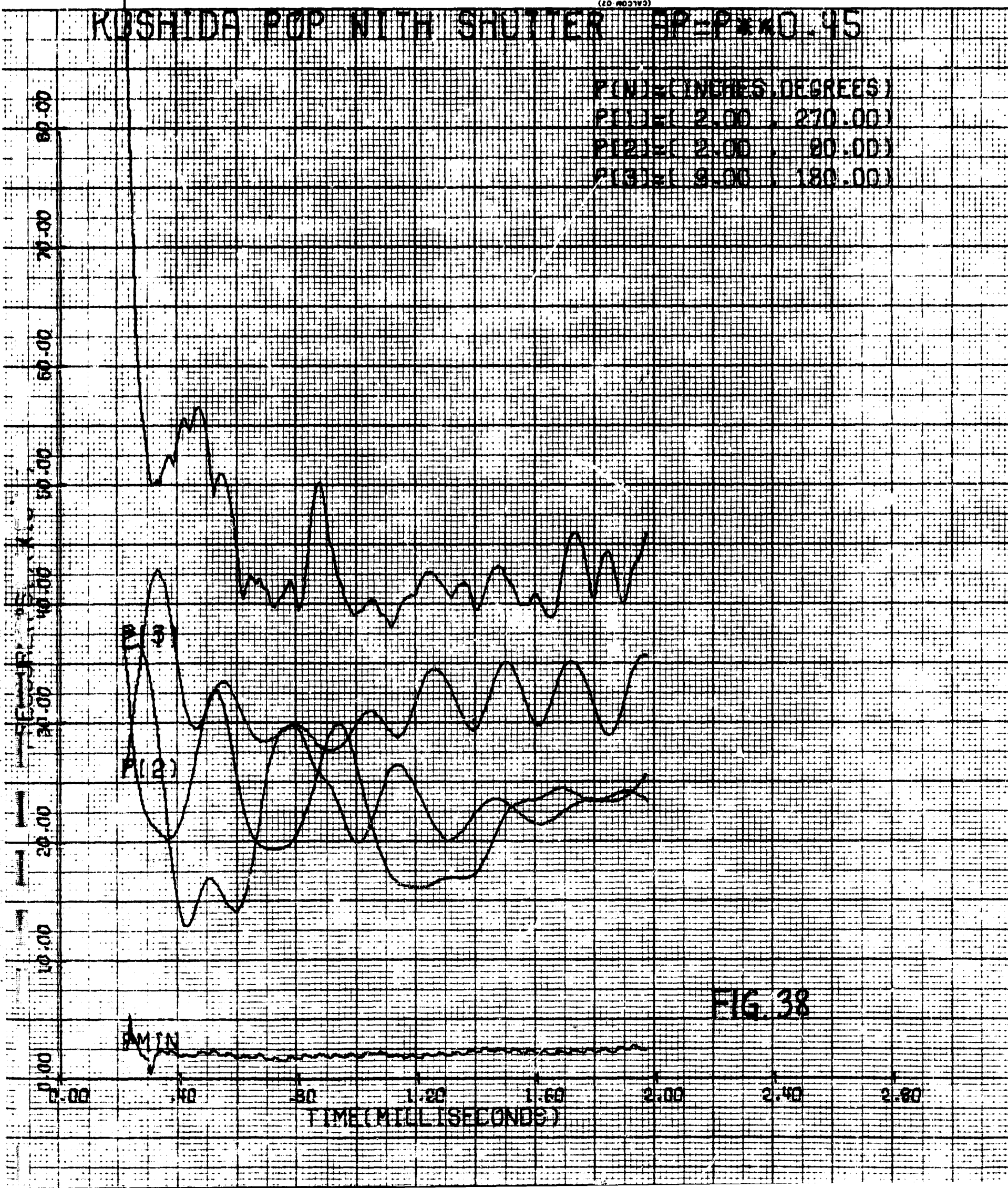

FIG. 38

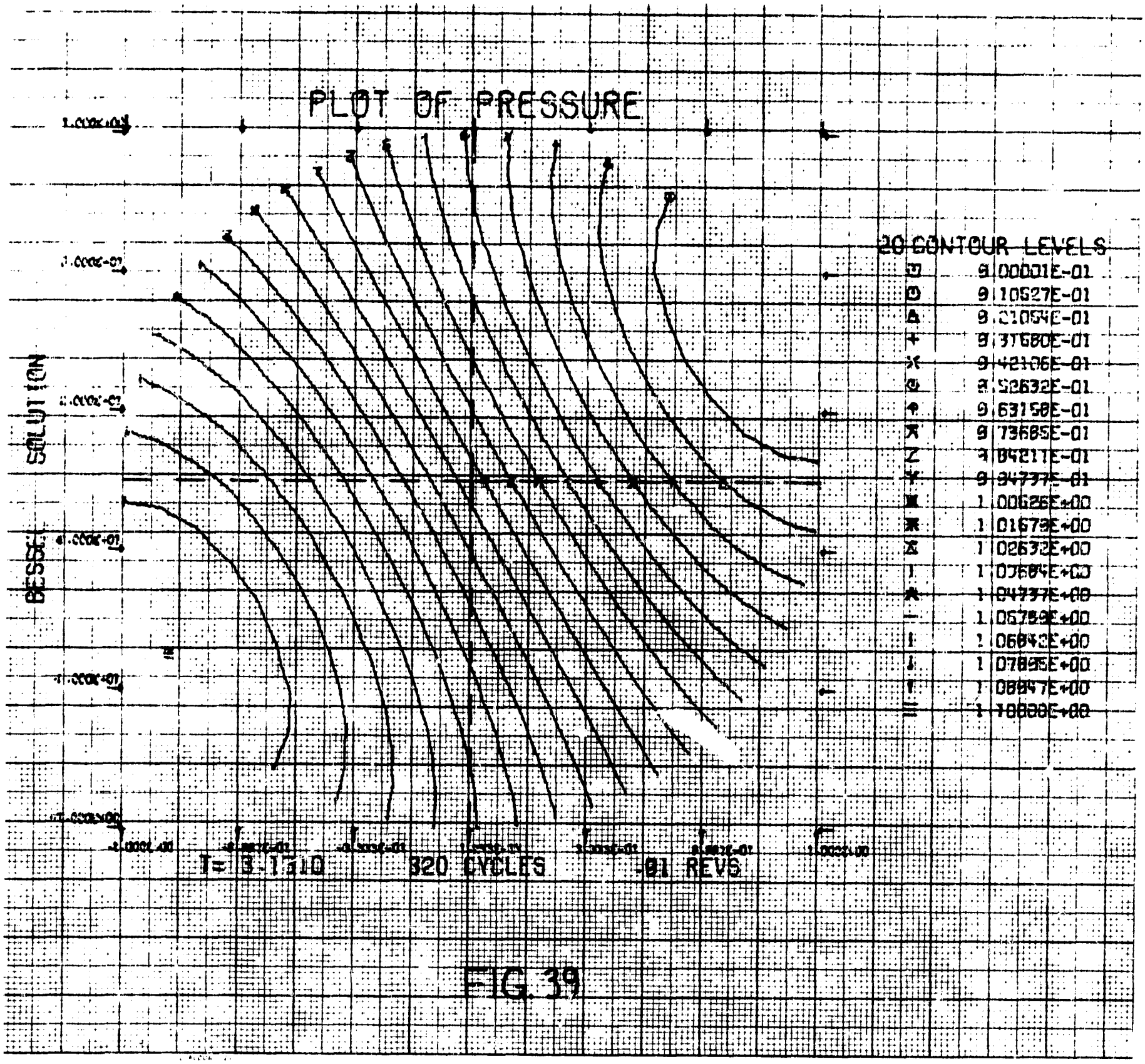

FIG. 39

PLOT OF PRESSURE

NUMERICAL SOLUTION $\frac{\partial p}{\partial r} = \frac{\rho v^2}{R}$

20 CONTOUR LEVELS

0	10232E-01
⊙	0 20862E-01
Δ	0 31403E-01
+	0 42123E-01
X	0 53253E-01
◇	0 63984E-01
↑	0 74014E-01
X	0 84644E-01
Y	0 95275E-01
Y	1 00591E+00
⊠	1 01664E+00
⊗	1 02717E+00
⊠	1 03780E+00
↑	1 04843E+00
★	1 05906E+00
—	1 06969E+00
↓	1 08032E+00
↓	1 08095E+00
↑	1 10160E+00
⊞	1 11221E+00

T= 3.1310 320 CYCLES 91 REVS

FIG. 40

(CALCO)

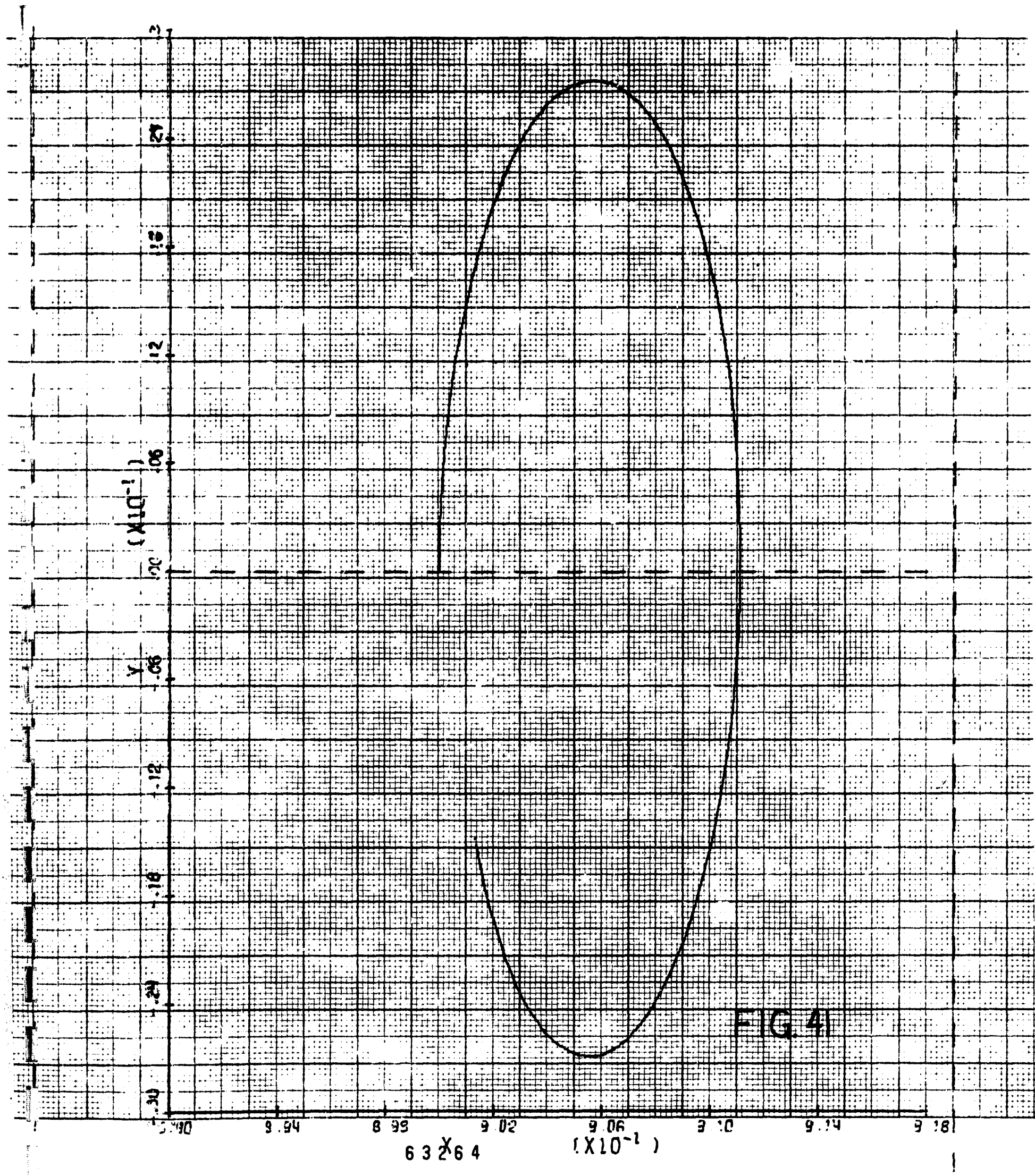

FIG. 41

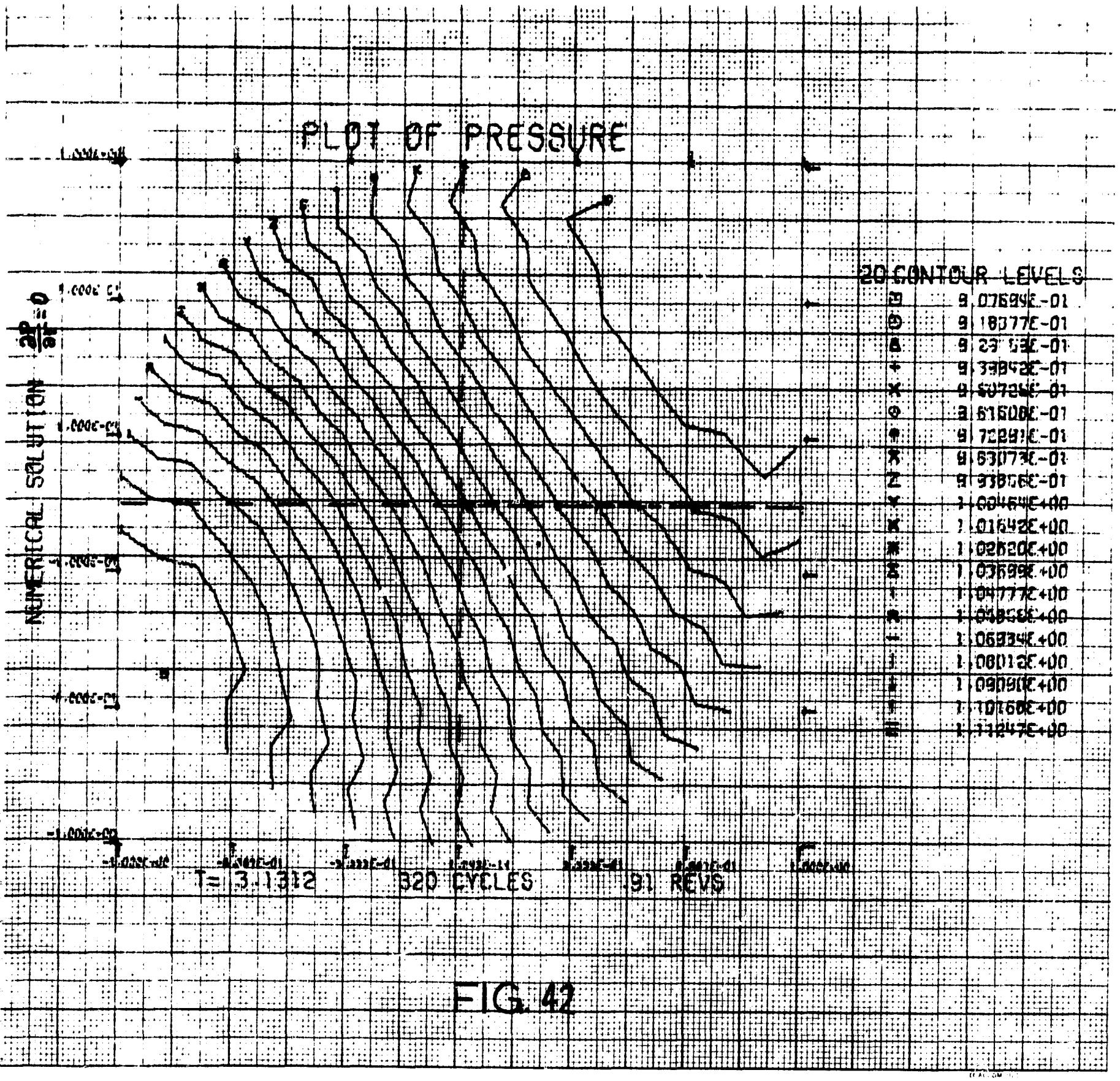
PLOT OF PRESSURE
NUMERICAL SOLUTION $\frac{\partial P}{\partial r} = 0$
20 CONTOUR LEVELS
T= 3.1312
320 CYCLES
91 REVS

FIG. 42